Aerodynamics and Control Aspects of Formation Flight for Induced Drag Savings

Technical Report · April 2019

DOI: 10.13140/RG.2.2.33983.12962

1 author:

Omid Bidar
The University of Sheffield
11 PUBLICATIONS **28** CITATIONS

Aerodynamics and Control Aspects of Formation Flight for Induced Drag Savings

Omid Bidar

The University of Sheffield, UK
&
University of Michigan, Ann Arbor, USA[*]

April 25, 2019

Abstract

Reduction of the carbon emissions due to commercial aviation, and fuel efficiency in general, is a key challenge the aerospace community is attempting to tackle. Formation flight is one of the potential solutions, which involves considerable fuel reductions due to induced drag savings. The present paper presents a) an extensive survey of current literature on aerodynamic analysis of formation flight, both theoretical (analytical and numerical) and experimental (wind tunnel and flight tests); b) a brief discussion of the proposed automated control systems in previous studies; and c) a study of six symmetric formation configuration using the single horseshoe vortex wing model to determine the optimum formation geometry. The detailed review, not previously reported in literature, shows that formation flight is a relatively extensively researched topic, with promising theoretical and experimental results. Simulations of the symmetric geometries give some insight into induced velocities on any given aircraft within a formation with respect to changes in lateral and longitudinal spacings, but application of systematic optimisation techniques is recommended for conclusive results.

Keywords: Formation flight; Induced drag savings; Aerodynamics; Automated control; Formation configurations; Commercial aviation

[*]This research was conducted as part of a Directed-Study course at the Department of Aerospace Engineering, University of Michigan, on a Global Engineering Education Exchange programme.

Contents

List of Figures **3**

1 Introduction **6**
1.1 Why is formation flight interesting? . . . 6
1.2 Major themes in the study of formation flight . . . 6
1.3 What to expect in this report? . . . 6

2 Theoretical Aerodynamic Analyses **6**
2.1 Single Horseshoe Vortex . . . 7
2.2 Unrolled Vortex Sheet . . . 9
2.3 Rolled-up Vortex Sheet . . . 11
2.4 More Complex Approaches . . . 13
2.5 Concluding Remarks . . . 14

3 Experimental Studies **14**
3.1 Flight Tests . . . 14
3.2 Wind Tunnel Experiments . . . 14

4 Automated Control **15**
4.1 Why is automated control critical? . . . 15
4.2 Design Process for a "Leader-Wingman" Formation . . . 15
4.3 More Complex Approaches . . . 18

5 Formation Configurations: An Application of the Theory **19**
5.1 Motivation . . . 19
5.2 Simplifications . . . 19
5.3 Governing Equations . . . 19
5.4 Geometries . . . 21
5.5 MATLAB Implementation . . . 22
5.6 Verification . . . 22
5.7 Results . . . 23
5.8 Discussion . . . 27

6 Conclusions and Future Work **28**

7 Appendices **28**

References **31**

List of Figures

1 Single horseshoe vortex wing model . . . 7
2 Vortex sheet wing model . . . 9
3 Vortex lattice method panelling . . . 10
4 Vortex sheet roll-up . . . 11
5 Rolled-up vortex sheet analysis model . . . 12
6 Proposed procedure for CFD simulation of two aircraft . . . 13
7 Leader-wingman formation block diagram, symbols, and frame of reference . . . 16
8 Induced velocity due to a vortex segment. . . . 19
9 The six formation configurations to be simulated for this study. . . . 21
10 Simulation process flow diagram . . . 22
11 Geometry used for code verification. . . . 23
12 Total downwash for various lateral spacings with constant longitudinal spacing . . . 23
13 Downwash on individual aircraft for V formation . . . 24
14 Downwash on individual aircraft for inverted-V formation . . . 24
15 Downwash on individual aircraft for W formation . . . 25
16 Downwash on individual aircraft for diamond (version 1) formation . . . 25
17 Downwash on individual aircraft for diamond (version 2) formation . . . 26
18 Downwash on individual aircraft for in-line formation . . . 26

Nomenclature

α	aspect angle
α_0	sectional lift curve slope of the wing
α_g	geometric twist of the wing
α_i	induced angle of attack
α_∞	aircraft angle of attack
$\alpha_{L=0}$	zero-lift angle of attack
δ	longitudinal vortex strength
η	position in the lateral direction on an infinitesimal lifting surface
Γ	vortex strength
γ	lateral vortex strength
ψ	heading angle
ρ	density
τ	time constant
$\hat{\mathbf{i}}$	unit vector in the stream-wise/longitudinal direction
$\hat{\mathbf{j}}$	unit vector in the spanwise/lateral direction
$\hat{\mathbf{k}}$	unit vector in the vertical/upward-lift direction
$\mathbf{F}$	force
$\mathbf{r}$	position of point of interest from vortex line
$\mathbf{v}_0$	induced velocity at centre of wing
$\mathbf{V}_\infty$	free-stream velocity
ξ	position in the longitudinal direction on an infinitesimal lifting surface
A	transition matrix
B	control input matrix
b	wingspan
C	output matrix
c	chord length
D	disturbance vector
D_i	induced drag
dl	infinitesimal vortex segment
h	distance from point of interest to a vortex

k	gain
L	lift
l	slant range
S	planform wing surface
U	input vector
U_∞	velocity in the $\hat{\mathbf{i}}$-direction
W	wake
w	induced velocity in the $\hat{\mathbf{k}}$-direction
X	state vector
x	stream-wise/longitudinal position
Y	output vector
y	position along the wingspan

1 Introduction

1.1 Why is formation flight interesting?

The phenomenon of flying in a formation exists in nature as observed in the flight of migrating birds, e.g. [1]; has applications in various sports (drafting/slipstreaming), e.g. [2]; and has also been studied and applied in aerospace, e.g. [3, 4]. Although the reason behind this in the case of avian flight is attributed to good optical relations and improved communications [5], power efficiency [6], or a combination of the two [7], for atmospheric human flight the interest is primarily in the reduced power requirement. This is not only crucial from the cost-savings perspective, but can also contribute to reducing emission levels for environmental protection.

1.2 Major themes in the study of formation flight

The reduction of power requirement can be explained by the reduction of the induced drag when flying in a formation. As a wing flies, it generates upwash. The flight of individual wings in the upwash generated by a system of wings lead to a reduced power requirement, or more accurately described as induced-drag savings.

While motion in a formation is a multi-disciplinary area of study that interests the biologist and the aerodynamists alike, the major themes in aerospace application is the investigation of the aerodynamics and control aspects of aircraft flying in formation. The two are closely linked as studies have shown that the degree to which induced-drag savings can be achieved has strong dependence on characteristics of each aircraft and the configuration of the formation*.

As this report develops, it will also become clear that with more detailed investigations in modelling the aerodynamics and controls aspects, implementations of formation flight in the commercial context should also be investigated.

1.3 What to expect in this report?

In Section 2, this report looks in some detail at the aerodynamics investigations of formation flight thus far. Beginning with earlier simpler analyses, the underlying assumptions, simplifications, and the outcomes, to more complex analyses enabled by advances in aerodynamic theory, computational fluid dynamics, and computational resources accessibility. Section 4 explores some aspects of implementing an automated control system by looking at existing literature.

Through a simplified model, we investigate formation configurations in Section 5. Beginning by motivating the need for this analysis, we formulate the problem mathematically, implement a computer program, and simulate for various geometries, followed by a report and discussion of the results.

Finally, some overall conclusions are drawn in Section 6, with some commentary on future work in the investigation of formation configurations.

2 Theoretical Aerodynamic Analyses

In order to understand the aerodynamics of multiple aircraft flying in a formation, an understanding of a single finite-wing is essential. To motivate this, we briefly return to explaining how lift is generated. In a sentence, lift is generated due to a pressure difference between the top and bottom surface of a wing - low pressure at the top, high pressure at the bottom. A by-product of this pressure difference is the curling of flow near the wing tips. This circulatory motion downstream of the wing, is aptly termed a *trailing vortex*. The wingtip vortices cause a downwash component of air velocity in the neighbourhood of the wing, called the *induced velocity*. It is this induced velocity that aircraft flying in a formation can exploit

*In this report we use the term *configuration* with the phrase *formation geometry* interchangeably.

to reduce induced drag. Therefore, the aerodynamic analysis of aircraft flying in formation is primarily concerned with the interactions of wing trailing vortices and their implications on the induced velocities.

The finite-wing aerodynamics is generally concerned with downwash, induced drag and effective angle of attack. Other tools required for the analysis are vortex filaments; Biot-Savart law and Helmholtz's vortex theorems. For details, see reference [8]. Henceforth, the term wing and finite-wing are used equivalently.

2.1 Single Horseshoe Vortex

The first attempt at the analysis of aerodynamics of formation flight was made by Wieselsberger, in 1914 [9]. Employing Prandtl's lifting-line theory[†], he studied flight of three birds in a diagonal formation using horseshoe vortices. This involves representation of the vortex on each wing with three parts: two counter-rotating trailing portions and a bound portion, hence the name, Figure 1. The vortex is defined by its strength, Γ.

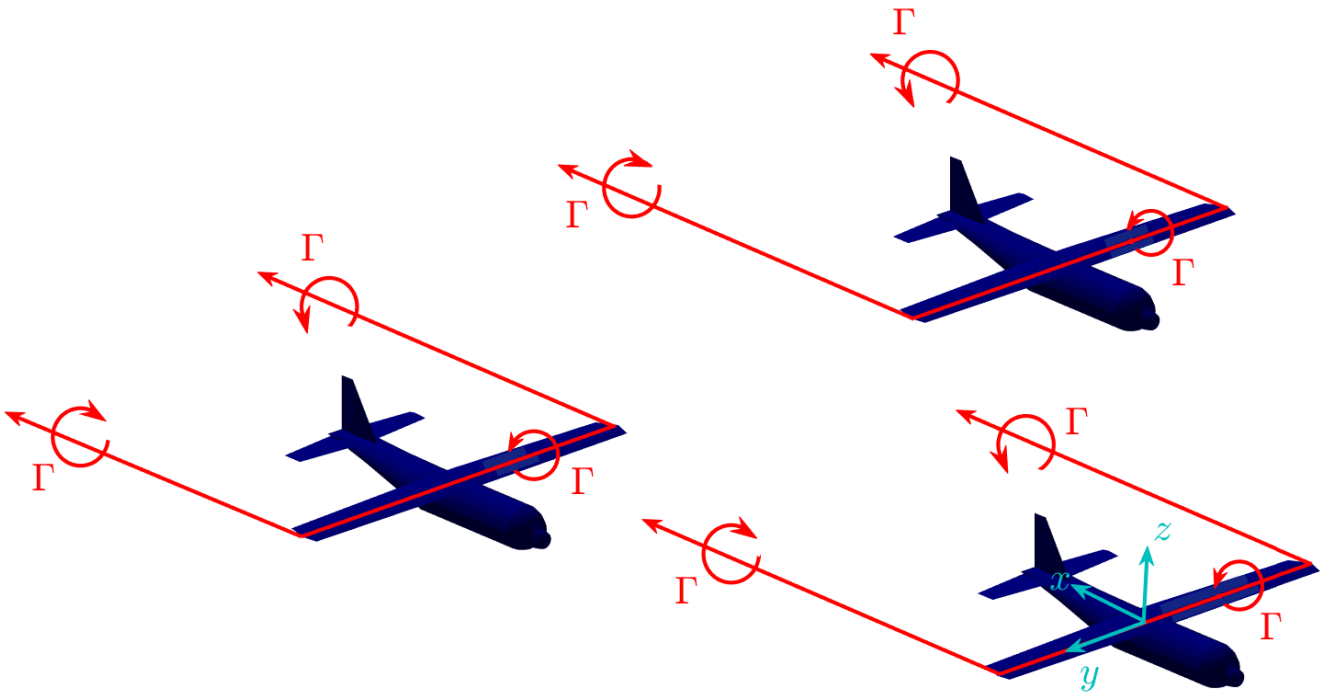

Figure 1: A single horseshoe vortex wing model.

In order to quantify effects of formation flight, the goal is to find the forces on the wings, based on the single horseshoe model. For this we look at the velocity in the middle of the bound vortex on each wing. Then the force can be approximated based on the three-dimensional generalisation of the Kutta-Joukowski theorem:

$$\mathbf{F} = \rho b \Gamma \mathbf{v}_0 \times \hat{\mathbf{j}}, \tag{1}$$

where the force, $\mathbf{F}$, on a wing is a function of the air density ρ, the wing span b, the vortex strength Γ, and the velocity at the centre of the wing $\mathbf{v}_0$. The force vector will have two components, in the $\hat{\mathbf{k}}$ and

[†]Wieselsberger was a doctoral student of Prandtl at the time [10], and was using recently developed theories by Prandtl, which means that the interest in formation flight is as old as the classical theory of lift generation.

$\hat{\mathbf{i}}$ directions, based on the coordinate system in Figure 1, corresponding to lift and induced drag forces respectively.

The velocity $\mathbf{v}_0$ incorporates the free-stream velocity, $\mathbf{V}_\infty$ and the velocities induced by the vortices. These induced velocities are due to the trailing portion of the horseshoe vortex modelling the aircraft under analysis, and the induced velocities due to the neighbouring aircraft. Computation of induced velocities involves the application of Biot-Savart law,

$$d\mathbf{v} = \frac{\Gamma}{4\pi}\frac{d\mathbf{l} \times \mathbf{r}}{r^3}, \tag{2}$$

which gives the velocity increment $d\mathbf{v}$ at any point due to a vortex segment as a function of the vortex strength Γ, a differential element of the vortex segment $d\mathbf{l}$ and position of the point of interest from the vortex line $\mathbf{r}$. The total induced velocity can then be calculated by integrating over the length of the vortex line. For detailed derivation see [8].

Following Wieselsberger's approach, many future formation analyses have employed a single horseshoe vortex wing model. Hummel, conducted numerous investigations in formation flight throughout late 1970s to 1990s, primarily with this model. For instance in [11] he studied the effects of different formation configurations with aircraft of identical characteristics (e.g. wingspan size), termed the *homogeneous*, and different characteristics, termed *inhomogenous*. His findings show that the total energy saving is highly dependent on the lateral spacing of the wings. For instance, in a V-formation, the trailing aircraft needs to fly as close to the wake of the lead aircraft as possible to achieve maximum upwash. On the other hand, the longitudinal distribution of the wings do not affect the overall drag reduction. However, it effects the distribution of the reduction among the individual aircraft in formation. For a V-formation the inner aircraft enjoy the most induced-drag reduction. The benefit decreases towards the apex and the edges as the aircraft in these position have no upwash (lead aircraft) from the neighbours or upwash from just one neighbour (trailing aircraft). The distribution can be improved by systematic modification of the shape of formation (further discussed in Section 5). For the inhomogenous case, wings with larger spans and higher weight than the other wings act in such a way that the neighbouring aircraft enjoy more induced drag reductions.

Similar effects had been observed earlier by Lissaman and Shollenberger in 1970, by examinations of bird flight [6]. They opted for analysis of bird flight due to the 'greater aerodynamic freedom of animal flight' as they considered aircraft formation flight impractical at the time due to 'dangerously close formation' requirements. The authors estabilshed a fixed-wing analog to allow analysing the bird as a fixed-wing aircraft by assuming small time-dependent perturbations around a steady state[‡].

Interestingly, it has been argued that for investigations of avian formation flight the flapping-wing nature of flight should be considered, as the fixed-wing assumptions lead to over-prediction of the induced drag reduction [13].

While a relatively simple model to implement, a single horseshoe vortex wing model assumes constant circulation, $\Gamma(y)$, and therefore constant lift distribution along the span. This is not the case with real wings as the pressure between the top and bottom surfaces of the wing equilibrates at the wing tip so that the circulation is zero. Additionally, a constant circulation is neither structurally, nor aerodynamically optimal because it will cause large bending moments at the root of the wing due to high tip loading, and will produce a lot of drag. Also, the horseshoe model only captures the wing span as far as wing geometry is concerned, which is very simplistic.

[‡]In a 2005 paper on simplified analytical methods for formation flight [12], Lissaman recalls the implementation of their study: "...using the most advanced computer technology of the time, the IBM 360. This computer was far from a laptop or a desktop, in fact it required a building the size of a four-unit apartment, so might have been called an 'earthtop computer'." This gives interesting context to the authors' reasoning to opt for avian formation flight.

2.2 Unrolled Vortex Sheet

To overcome the limitations of the single horseshoe vortex wing model, it is required to *shed* vorticity along the wing span, leading to the vortex sheet model. This is as a result of Helmholtz's first theorem which states that the strength of a single vortex line cannot change, again refer to [8] for details. Figure 2 shows a vortex sheet model of a wing, with non-constant circulation $\Gamma(y)$ along the span.

The vortex sheet is also called the wake. Prandtl's classical lifting-line theory can be used to characterise the wake, by constructing it as a superposition of an infinite number of vortex lines, with strengths $d\Gamma$.

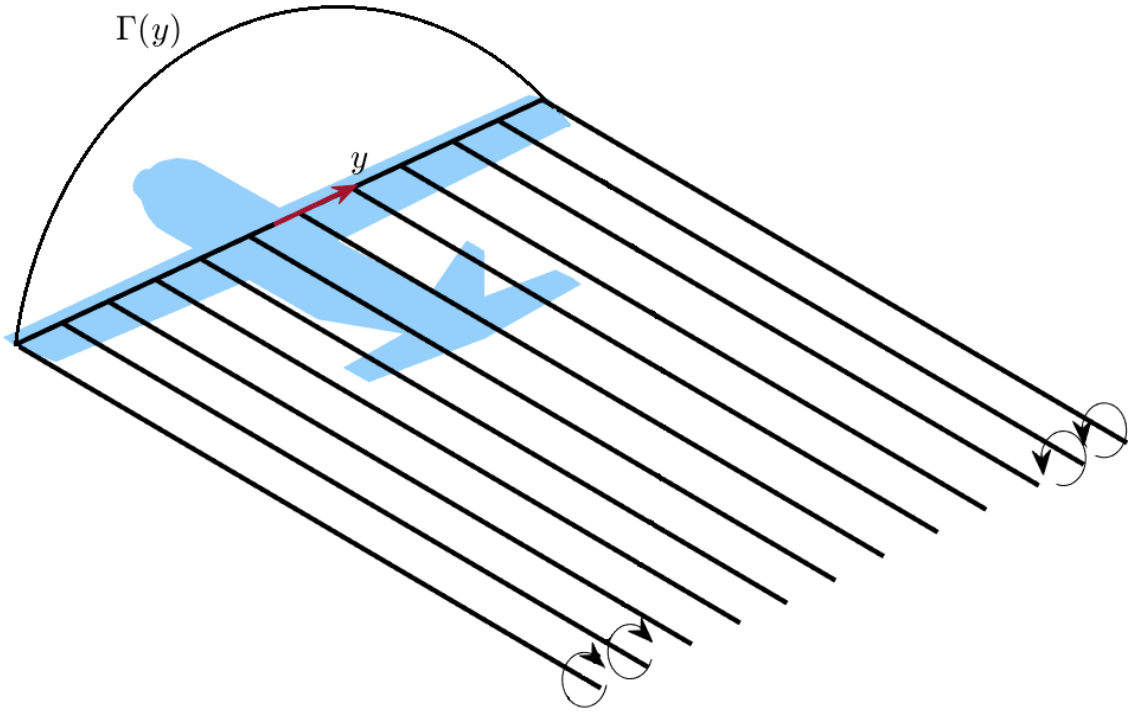

Figure 2: A vortex sheet wing model with shed vorticity, assuming that it convects downstream in the x-direction.

The vorticity shed between y and $y + dy$ is $d\Gamma = (d\Gamma/dy)dy$. By employing the Biot-Savart law, the downwash at an arbitrary point y_0 along the span can thus be calculated as

$$w(y_0) = -\frac{1}{4\pi}\int_{-b/2}^{b/2} \frac{(d\Gamma/dy)dy}{y_0 - y}, \tag{3}$$

where b is the wing span.

The lift and induced drag forces can then be calculated by the application of Kutta-Joukowski theorem to find the sectional forces, and intergrating over the span:

$$L = \rho \mathbf{V}_\infty \int_{-b/2}^{b/2} \Gamma(y)dy \qquad D_i = \rho \mathbf{V}_\infty \int_{-b/2}^{b/2} \Gamma(y)\alpha_i(y)dy \tag{4}$$

where α_i defined as $-w(y_0)/\mathbf{V}_\infty$ for small angles, is the induced angle of attack which accounts for the deflection of local airflow around the wing as a result of the downwash.

One approach to analyse wings with the model outlined above is to use the *fundamental equation of Prandtl's lifting-line theory*, with several assumptions. The assumptions are steady, potential flow[§],

[§]Implying it is assumed that the flow is inviscid, irrotational, and incompressible.

high aspect ratio and low sweep angle wing, no crossflow, and most importantly, flat wake. We return to the last assumption later. Although, the detailed derivation of this equation is beyond the scope of this report, it is shown below to illustrate the approach for aerodynamic analysis of wings flying in formation:

$$\alpha_\infty + \alpha_g(y_0) = \frac{2\Gamma(y_0)}{\alpha_0(y_0)U_\infty c(y_0)} + \alpha_{L=0}(y_0) + \frac{1}{4\pi U_\infty}\int_{-b/2}^{b/2}\frac{d\Gamma/dy}{y_0 - y}dy \tag{5}$$

where α_∞ is the aircraft angle of attack, α_g is the geometric twist of the wing, α_0 is the sectional lift curve slope of the wing, $\alpha_{L=0}$ is the zero-lift angle of attack; $c(y_0)$ is the sectional chord length and U_∞ is the speed in the $\hat{\mathbf{i}}$-direction. Solving Eqn. 5 requires solving an integro-differential equation, to compute $\Gamma(y_0)$, from which the forces can then be calculated. The *point collocation* is one approach to solve this equation by enforcing it at a finite number of points. For the details of this process see [8].

Although the point collocation method is relatively simple to apply for analysis of a single wing, the analysis of multiple wings and the wake interactions becomes complex. Various other numerical techniques can be used to perform this analysis instead. The *vortex lattice method* is one such approach. In the

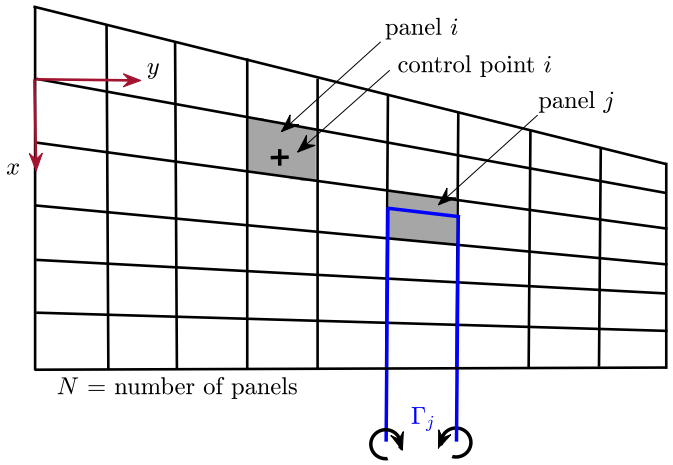

Figure 3: The vortex lattice method: panelling and horseshoe vortex placement for a right wing.

vortex lattice method a wing is divided into quadrilateral panels. A horseshoe vortex is placed on each panel with the bound portion on the quarter-chord line of the panel and the trailing vortices extending to infinity in the x-direction. Control points are then placed on each panel and flow tangency is enforced at each control point as follows:

$$w_i + U_\infty\left(\alpha_\infty + \alpha_{\text{panel}i}\right) = 0, \tag{6}$$

where w_i is induced downwash at the control point i, U_∞ is the flow speed in the x-direction, α_∞ is the wing angle of attack, $\alpha_{\text{panel}i}$ is the local angle of attack of panel i which includes the wing geometry information (i.e. geometric twist and camber). A linear system is set up based on Eqn. 6 to compute the circulations on each panel as follows:

$$w_i = \sum_{j=1}^{N} A_{ij}\Gamma_j, \tag{7}$$

where the index i represents the control points and j represent the panel, and N is the total number of panels. A_{ij} captures the influence coefficients of panel j on control point i and is only a function of the wing geometry.

As it clear from the terms in the equations developed thus far, it is clear that with an unrolled vortex sheet model we can capture wing geometry effects, such as camber and geometric twist, while in the single horseshoe model the wing is primarily modelled by the span only. With non-constant circulation along the wing $\Gamma(y)$ the wing is more realistically represented, and rolling moment due to asymmetrical upwash

distribution can be computed. With this, appropriate aileron deflections can be employed to compensate for the produced rolling moment, which the single horseshoe vortex model fails to capture.

Many codes are available to perform this numerical analysis. For instance, [14] employed the HASC95 code developed by NASA [15]. An alternative software, commonly used at educational institutions, is Athena vortex lattice (AVL), developed by Drela and Youngren, which models lifting surfaces using the unrolled-vortex sheet model [16].

For large lateral distance between aircraft in formation, results with this model are reported to show very similar trends to those obtained from the horseshoe model. But for very low lateral distances, where the wake interactions effects are more pronounced, the horseshoe model underestimates the induced drag reductions [14, 17]. With very close lateral distances, up to one tenth of a wing span, ranges increases of sixty percent are reported for a five aircraft formation [14].

Maximum induced drag reductions can be achieved by strategically flying in the wake of an aircraft. This leads to very small lateral distances between aircraft, or even the overlap of wings, laterally. Therefore, the *unrolled* vortex sheet representation is more appropriate compared to the horseshoe model. But, the wake of real wings tend to roll-up, and yet again, another layer of sophistication in the model is required to capture this effect. For simplified unrolled-vortex sheet analysis of aircraft in a horizontal plane it can be assumed that the wake is kept flat and straight by external side-forces acting laterally, y-direction in Figure 1. For lift and induced drag forces in z and x-direction respectively, there is no contribution of these sides forces, hence the solutions will still be valid.

2.3 Rolled-up Vortex Sheet

The tips of a real vortex sheet tends to roll up, as shown in Figure 4, due to velocities in the z and y direction induced by the wake on itself. This is called *force-free* wake [18].

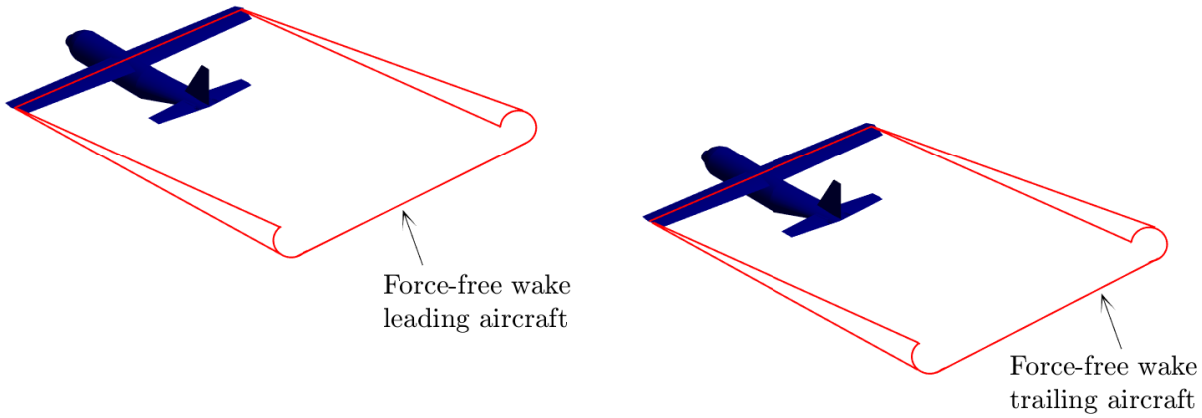

Figure 4: A more accurate wake representation, where the vortex sheet rolls up. This is called the force-free wake.

The complexity this effect produces in the model is illustrated by the following equation, derived in [8], based on the lifting-line theory:

$$w(x,y) = -\frac{1}{4\pi}\iint_S \frac{(x-\xi)\gamma(\xi,\eta)+(y-\eta)\delta(\xi,\eta)}{[(x-\xi)^2+(y-\eta)^2]^{3/2}}d\xi d\eta - \frac{1}{4\pi}\iint_W \frac{(y-\eta)\delta_w(\xi,\eta)}{[(x-\xi)^2+(y-\eta)^2]^{3/2}}d\xi d\eta \qquad (8)$$

where the induced velocity $w(x,y)$ at any point on a wing requires evaluating a double-integral over the planform wing surface S and, the wake W, Figure 5. ξ and η denote the positions in the x and y directions of an infinitesimal segment of the lifting surface (i.e. wing); γ is the lateral vortex strength, and δ is the

longitudinal vortex strength, and both are a function of x and y. δ_w is the vortex strength of the wake in the y direction. Eqn. 8 can be solved numerically, by adapting the vortex lattice method described in

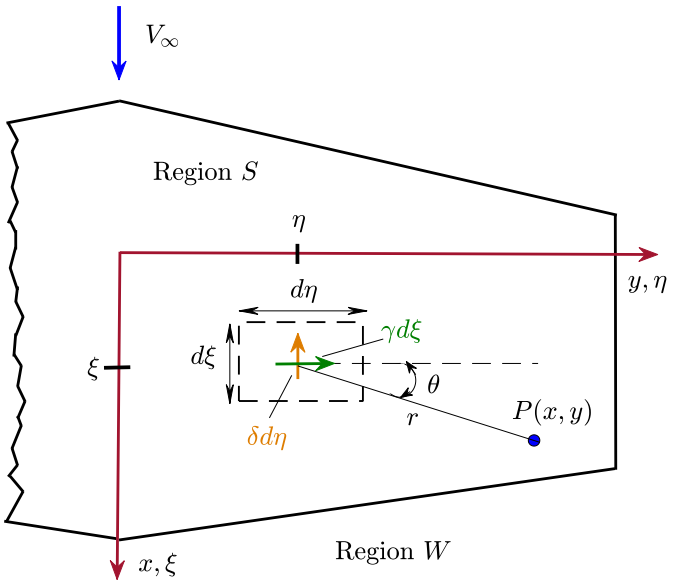

Figure 5: Velocity induced at point P by an infinitesimal segment of the lifting surface, the velocity is out of page. Based on figure 5.34 from [8].

Section 2.2. This involves an iterative process where the trailing vortices applied at the quadrilaterals are initially assumed to be semi-infinite in the x direction, then the trajectories of these vortices are calculated iteratively to simulate a force-free wake.

The technique above was applied by Maskew in 1974 to study a three aircraft formation [19]. The author reports a potential aircraft range increase due to the formation to be between 46% to 67%. He also investigated various formations, with zero lateral spacing between the aircraft wing tips and three wingspan longitudinal spacings. For the V formation an 80% induced drag reduction has been reported on all but the lead aircraft. For a double-row formation there is virtually no induced drag savings on the leading aircraft, but the aircraft in the second row have an induced thrust of 48% of their free-air induced drag.

Various other rolled-up wake models have been developed over the years. Some of these models simplify the problem by neglecting viscous effects during the rollup phase, as the process is typically very rapid, and the wake velocities can be considered as a two-dimensional flow. These model begin by an assumption on the vorticity distribution. For instance, the simplest model concentrates all the vorticity at one point, however this leads to singularity at one point with infinite kinetic energy, which is problematic [3]. To overcome this issue, the vorticity can be distributed differently. One such model is the Rankine vortex, with uniformly distributed vorticity over a circular region [20]. Another model is the Lamb-Oseen vortex, which assumes an exponential decay in the swirl velocity. But these models rely on other methods to compute the core size (radius of peak velocity). Prandtl proposed one method to choose the core size which is based on the conservation of mechanical energy applied over a large control volume containing the aircraft. The induced drag is assumed to be approximately equal to the kinetic energy of the fluid in the Treftz plane [21]. The details of these analyses and their limitations are beyond the scope of the present study. Some cited literature on these are: [22–27].

Results from these analyses are presented by reporting findings of [3, 28, 29], three of the recent publications applying forms of the techniques above.

In [28], the authors model two aircraft in formation, each approximately modelled as the Standard Cirrus saleplane. The span efficiencies are used as a metric of the formation benefits. The main findings show that a maximum span efficiency greater than 3.0 is achievable by the follower aircraft when the

wings overlap, laterally, to 10-25% of their spans. [29] uses the AVL program, by adapting it to model wake-rollup effects. The aircraft in formation is based on a complete A330-like model. By using previously found spacing for maximum induced-drag reduction from [14][¶], the authors show that if the induced drag in cruise is assumed to be around 40% of the total drag, the potential drag saving for an A300-like model is around 13%. Control surfaces deflections are also determined to achieve certain angles of attack for a particular flight condition for the formation.

The author of [3] conducts a more detailed analysis by not only considering wake roll-up effects, but also modelling vortex decay, vortex instabilities, vortex motion, and atmospheric turbulence. This paper is also one of the few that analyses purely *extended* formation flight (longitudinal spacing of multiple-tens of wing spans between aircraft), which reduces collision risks. In a two aircraft formation, for a longitudinal separation of less than 30 spans in low to moderately low turbulence levels, a maximum induced drag reduction of 30% $\pm$ 3% is reported for V, inverted-V and echelon formations.

2.4 More Complex Approaches

In addition to the models discussed so far, some recent literature have proposed multi-fidelity approaches, to analyse the aerodynamics of formation flight. For instance, in [30] two rectangular NACA23012 wings are modelled using both vortex lattice method, and a Reynolds Averaged Navier-Stokes (RANS) simulation in three-spatial dimensions. The authors consider incompressible flow in a fully turbulent regime, at a Reynolds number of 0.24×10^6 based on the chord. The shear-stress-transport (SST), $\kappa - \omega$ turbulence model is used to simulate the flow. Simulation results of both the VLM and RANS methods are compared against experimental results from [31]. The VLM method is found to over-predict the lift and drag, while the RANS models is reported to show good agreement with the experimental results. Similar comparisons are also shown in [32], where a hybrid computational fluid dynamics (CFD) model is used along with the VLM method.

Most of the models described thus far assume potential flow, (i.e. inviscid, irrotational, and incompressible). However, for aircraft flying in transonic regimes, compressibility effects can lead to additional drag [33]. This is especially true for the trailing aircraft as the load changes considerably due to the upstream wake and the need for appropriate control surfaces deflections in order to trim. In this case even more sophisticated calculations are required.

For extended formation flight, [34], a compressible CFD simulation for two aircraft is proposed, with procedure shown in Figure 6. As CFD simulations are computationally expensive, for aircraft sufficiently far apart, the analysis is decoupled into three phases.

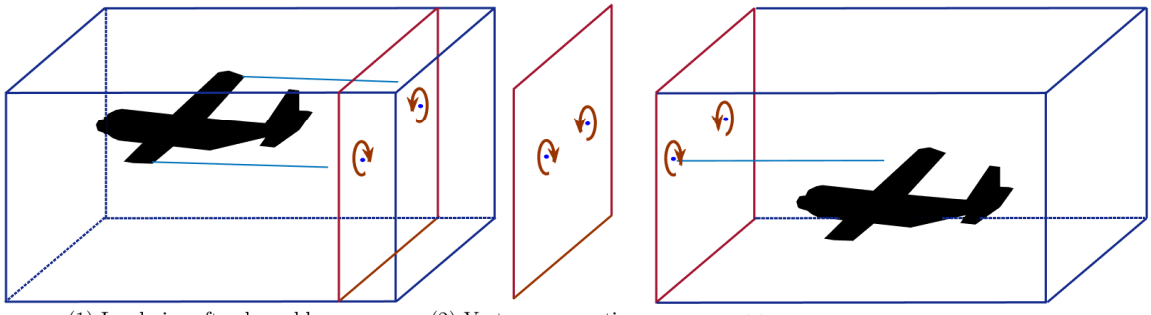

Figure 6: Proposed analysis procedure for two aircraft in extended formation flight, adapted from [34].

[¶]The authors present a plot showing contours of induced-drag reduction of a following aircraft, for various vertical and lateral spacings. The so-called sweet spot is shown to be the following spacing between the centerlines of the wings: vertical spacing (z direction in reference coordinates of Figure 1) of 40% of the span, and lateral (y direction) of 50% of the span. For details refer to [14].

In phase (1) the lead aircraft is simulated in the free flow using the Euler solver; in phase (2) the wake propagation of the lead aircraft is modelled using an augmented Betz model; in phase 3) the flow on trailing aircraft is simulated with the aged wake/vortex at the inflow boundary. Results of inviscid drag savings on the trailing aircraft show that for roll trim at transonic conditions 15% of the benefits are lost. Overall, the trail aircraft save 54% in induced drag in subsonic flow, and 35% in transonic flow when trimmed in roll.

2.5 Concluding Remarks

Various modelling methods are available to study the aerodynamics of formation flight. Sophisticated models are required in order to model the wake of the aircraft in the formation. For close formation flight especially, wake roll up effects should be considered. One of the commonly used methods is the vortex lattice method, due to its relative simplicity, accuracy and computational efficiency.

Unfortunately, there is no baseline case to compare results from various studies, and various metrics are used to measure formation flight benefits. However, all the analyses have shown that considerable induced drag savings are achievable.

3 Experimental Studies

Apart from the theoretical analysis, over the years, some flight tests and wind tunnel experiments have also been conducted. Findings are breifly described in this section.

3.1 Flight Tests

Hummel and Beukenberg performed one of the first flight tests of two Do-28 aircraft [35] in 1990. Flight test results were reported to show excellent agreement with the theoretical predictions. For zero lateral distance between the aircraft wing tips, the trailing aircraft obtained a 15% power reduction. Observations also showed that with increasing lateral distances, the benefits decreased rapidly.

Funded by NASA's Revolutionary Concepts Program, the Autonomous Formation Flight Project conducted flight tests of two F/A-18 aircraft in 2001 [36–38]. They demonstrated that a maximum 18% fuel saving is obtainable. Wagner and Blake report an 8% average fuel saving of the trailing aircraft for a two T-38 Talon aircraft, with lateral wing overlap of around 3.5 feet [39]. In the study of larger transport aircraft in 2012, Pahle and Berger have observed a maximum fuel savings of 6.8% to 7.8% for two C-17 aircraft [40]. More recent NASA flight tests for two business jets, Gulfstream C-20A (lead aircraft) and Gulfstream III (trail aircraft), have shown consistent fuel savings of over 2%. However, two test points that went significantly beyond the threshold ride quality, showed sustained fuel flow reduction of 3.5% to 8%, with momentary savings as high as 10% [41] [‖].

3.2 Wind Tunnel Experiments

Blake and Gingras conducted wind tunnel tests of two delta wing aircraft in close formations in 2002 [42] and compared the experimental results to VLM-based predictions [14]. For larger lateral and vertical spacings, the results show good agreement with theoretical predictions. For the cases where wings overlap in the lateral direction, theoretical results over-predict the induced-drag benefits. The trailing aircraft induced drags are reduced most when the wing tips of the two aircraft are aligned or slightly overlap. For wing tip overlaps of greater than half of the span, drag increases. The maximum induced drag reduction of

[‖] The authors clarify that the main objective of this experiment was to demonstrate moderate benefits with civilian aircraft using Automatic Dependent Surveillance-Broadcast (ADS-B) navigation, so these results do not necessarily represent the maximum achievable benefit.

25% is measured on the trail aircraft, with the wing tip overlap of 15-20% span, compared to a predicted 40% reduction with 10% overlap from the VLM analysis.

Inasawa et al., have performed wind tunnel experiments of two NACA 23012 airfoil more recently [31]. They have shown that for a logitudinal spacing of 2.5 times the wing chord, and wing tip overlap of 5% of the span, the lift-to-drag ratio was increased by approximately 24% compared to the isolated wing in the absence of the lead wing. Wind tunnel experiments for micro air vehicles (MAVs) at low Reynolds numbers have also reported a 14% power reduction for two-wing formation, and 24% for three-wing formation for a wing overlap of 14% of the chord [43].

4 Automated Control

4.1 Why is automated control critical?

One of the first flight test experiments to study formation flight, conducted by Beukenberg and Hummel, reported difficulties faced by the pilot of the trailing aircraft to maintain the required flight conditions and precise separation from the lead aircraft simultaneously [35]. Similar handling issues are also reported in [41]. Formation flight involves flying through part of the wake left behind by a lead aircraft, which is regions of disturbed air. In order for the rear aircraft to maintain nominal flight conditions, appropriate control surfaces deflections need to be applied, which can be a daunting manual task for long-flights. Therefore, an automated control system is required to overcome this issue.

Beukenberg and Hummel, did just that, by implementing an adapted experimental three-axes autopilot [44] on the trailing aircraft to perform the flights, results previously outlined in Section 3.1. The autopilot controlled the longitudinal motion of the aircraft by locating the optimal configuration, and using the elevator and throttle as the control elements. In the following subsections we outline some of the control designs proposed and implemented**.

4.2 Design Process for a "Leader-Wingman" Formation

Some of the earlier formation flight control system designs were investigated at the Air Force Institute of Technology, [45–48]. These papers analyse the automated control of two aircraft, the 'leader-wingman' formation, based on proportional and integral compensation feedback systems optimised from pole-assignment arguments. It is assumed that conventional auto-pilot systems are already in place for the two individual aircraft to maintain heading, height and Mach hold, and the formation auto-pilot adapts these to achieve formation control. The auto-pilot is designed by considering the formation dynamics in the state-space equations of the wingman.

The formation controller is on the wingman and it is assumed that this aircraft has the appropriate sensors to track the leader. Both the aircraft are modelled as first-order systems, with the control system shown in Figure 7. In this particular model the controller inputs consist of the heading and velocity of the wingman and lead aircraft, the states of the latter treated as disturbance signals. The controller outputs are the heading angle and velocity for the wingman aircraft which is dictated by proportional and integral-based compensators within the controller.

Only horizontal formations are considered in order to simplify the analysis, leading to a 4-degree-of-freedom model. By placing the rotating frame of reference on the trailing aircraft as shown in Figure 7b, the perturbed states governing the motion are the longitudinal distance between the aircraft x, the lateral distance y, the heading ψ_W and the velocity V_W of the trailing aircraft. Thus the linear time invariant

**It is interesting to note that automated control of formation flight can hugely benefit from the extensive investigations conducted for other similar applications: aerial-refuelling, air traffic coordination within high density airspace, and mixed and swarm operations of unmanned aerial vehicles.

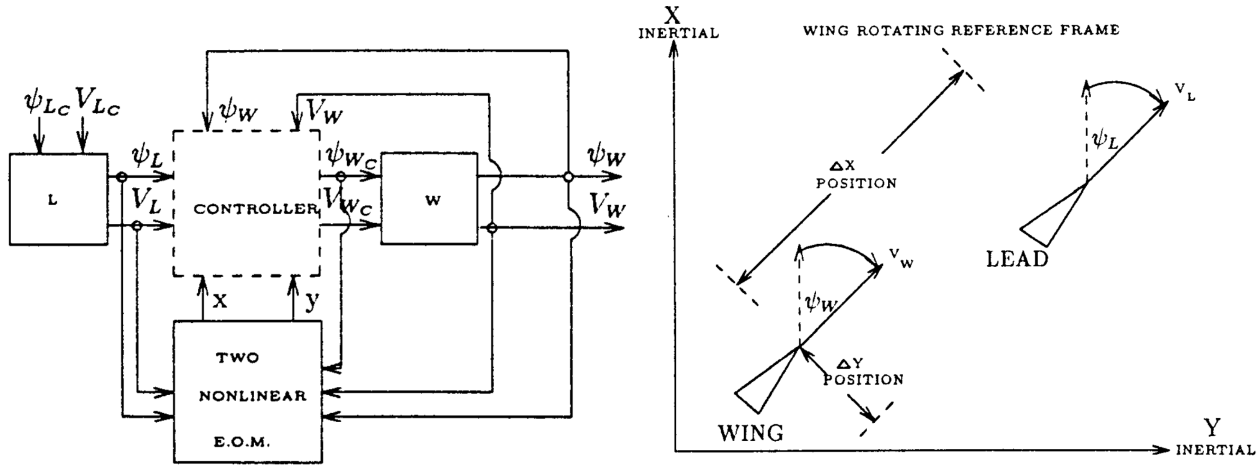

(a) **(b)**

Figure 7: (a) The formation control system proposed in [45–48], (b) the frame of reference. Symbols: L = lead aircraft, W = wing aircraft, c = command/input, V = speed, and ψ = heading angle. (Figure is from a paper that is declared a work of the U.S. Government and is not subject to copyright protection in the U.S.).

(LTI) equations of motion are:

$$\begin{aligned}
\dot{x} &= -\frac{y_0}{\tau_{\psi_W}}\psi_W - V_W + V_L + \frac{y_0}{\tau_{\psi_W}}\psi_{W_c}, \\
\dot{y} &= \left(\frac{x_0}{\tau_{\psi_W}} - V_0\right)\psi_W + V_0\psi_L - \frac{x_0}{\tau_{\psi w}}\psi_{W_c}, \\
\dot{\psi}_W &= -\frac{1}{\tau_{\psi_W}}\psi_W + \frac{1}{\tau_{\psi_W}}\psi_{W_c}, \\
\dot{V}_W &= -\frac{1}{\tau_{V_W}}V_W + \frac{1}{\tau_{V_W}}V_{W_c}.
\end{aligned} \tag{9}$$

where x_0, y_0 and V_0 are the nominal longitudinal separation, lateral separation, and formation velocity respectively, and τ_{ψ_W} and τ_{V_W} are the time constants for the heading and velocity of the trailing aircraft. The system can be parameterized with slant range $l = \sqrt{x_0^2 + y_0^2}$ and aspect angle α where $x_0 = l\cos\alpha$ and $y_0 = l\sin\alpha$. With these, Eqn. 9 can be written in state-space form as:

$$\begin{aligned}
\dot{X} &= AX + BU + \Gamma D, \\
\dot{Y} &= CX,
\end{aligned} \tag{10}$$

where X is the states vector, A is state transition matrix, B is the control input matrix, U is inputs vector; Γ is the disturbance matrix, D is the disturbance vector, Y is the output vector, and C is the output matrix. Substituting for these gives the following systems of equations:

$$\begin{bmatrix} \dot{x} \\ \dot{V}_W \\ \dot{y} \\ \dot{\psi}_W \end{bmatrix} = \begin{bmatrix} 0 & -1 & 0 & -\frac{\sin\alpha}{\tau_{\psi_W}} \\ 0 & -\frac{1}{\tau_{\psi_W}} & 0 & 0 \\ 0 & 0 & 0 & \frac{\cos\alpha}{\tau_{\psi_W}} - 1 \\ 0 & 0 & 0 & -\frac{1}{\tau_{\psi_W}} \end{bmatrix} \begin{bmatrix} x \\ V_W \\ y \\ \psi_W \end{bmatrix} + \begin{bmatrix} 0 & \frac{\sin\alpha}{\tau_{\psi_W}} \\ \frac{1}{\tau_{\psi_W}} & 0 \\ 0 & -\frac{\cos\alpha}{\tau_{\psi w}} \\ 0 & \frac{1}{\tau_{\psi_W}} \end{bmatrix} \begin{bmatrix} V_{w_c} \\ \psi_{W_c} \end{bmatrix} + \begin{bmatrix} 1 & 0 \\ 0 & 0 \\ 0 & 1 \\ 0 & 0 \end{bmatrix} \begin{bmatrix} V_L \\ \psi_L \end{bmatrix}, \tag{11}$$

$$\begin{bmatrix}\dot{x}\\ \dot{y}\end{bmatrix} = \begin{bmatrix}1 & 0 & 0 & 0\\ 0 & 0 & 0 & 0\end{bmatrix}\begin{bmatrix}x\\ V_W\\ y\\ \psi_W\end{bmatrix}. \tag{12}$$

For the compensator design, it is easier to decouple the states to $X = [(x, V_W), (y, \psi_W)]^T$, giving rise to the X- and Y-channels. This means that the trailing aircraft's heading command ψ_{W_c} responds to the lateral spacing y between the aircraft, and similar for the X-channel. For a representative design approach, we shall now focus on the Y-channel only. For detailed steps please refer to [48].

The goal now is to design a proportional and integral (PI) control that operates on the error for the lateral spacing, y. From the definition of a PI control, the trailing aircraft heading command is given by

$$\psi_{W_c} = k_{y_p} y + k_{y_i}\int_0^t y dt \tag{13}$$

where k_{yp} and k_{yi} are constant proportional and integral gains respectively. Differentiating Eqn. 13 and substituting for $\dot{y}$ in the resulting equation from Eqn. 9, we have

$$\dot{\psi}_{W_c} = k_{y_i} y + k_{y_p}\left(\frac{\cos\alpha}{\tau_{\psi_W}} - 1\right)\psi_W - k_{y_p}\frac{\cos\alpha}{\tau_{\psi_W}}\psi_{W_c} + k_{y_p}\psi_L. \tag{14}$$

Thus the augmented (i.e. including PI control) system of equation in state-space form for the Y-channel is,

$$\begin{aligned}\dot{X}_y &= A_y X_y + \Gamma_Y D_y,\\ \dot{Y}_y &= C_y X_y,\end{aligned} \tag{15}$$

$$\begin{bmatrix}\dot{y}\\ \dot{\psi}_W\\ \dot{\psi}_{W_c}\end{bmatrix} = \begin{bmatrix}0 & \frac{\cos\alpha}{\tau_{\psi_W}} - 1 & -\frac{\cos\alpha}{\tau_{\psi_W}}\\ 0 & -\frac{1}{\tau_{\psi_W}} & \frac{1}{\tau_{\psi_W}}\\ k_{y_i} & k_{y_p}\left(\frac{\cos\alpha}{\tau_{\psi_W}} - 1\right) & -k_{y_p}\frac{\cos\alpha}{\tau_{\psi_W}}\end{bmatrix}\begin{bmatrix}y\\ \psi_W\\ \psi_{W_c}\end{bmatrix} + \begin{bmatrix}1\\ 0\\ k_{y_p}\end{bmatrix}\psi_L, \tag{16}$$

$$\dot{Y}_y = \psi_W. \tag{17}$$

We can now analyse the system by considering the characteristic equation,

$$\det(sI - A_y) = \tau_{\psi_W} s^3 + (k_{y_p}\cos\alpha + 1)s^2 + (k_{y_p} + k_{y_i}\cos\alpha)s + k_{y_i} = 0. \tag{18}$$

and a Routh-array stability analysis can be performed to obtain constraints on the PI gains and time constants:

s^3	τ_{ψ_W}	$(k_{y_p} + k_{y_i}\cos\alpha)$
s^2	$k_{y_p}\cos\alpha + 1$	k_{y_i}
s^1	$\frac{(k_{y_p}\cos\alpha+1)(k_{y_p}+k_{y_i}\cos\alpha)-\tau_{\psi_W}k_{y_i}}{(k_{y_p}\cos\alpha+1)}$	
s^0	k_{y_i}	

$$\begin{aligned}\tau_{\psi_W} &> 0,\\ k_{y_p} &> -\frac{1}{\cos\alpha},\\ k_{y_p} + k_{y_i}\cos\alpha &> \frac{\tau_{\psi_W} k_{y_i}}{k_{y_p}\cos\alpha + 1},\\ k_{y_i} &> 0.\end{aligned} \tag{19}$$

The relations above can now be used to determine the various parameters based on the response behaviour required for the formation control system, with pole placement as one of the techniques, for details and results refer to the cited papers[††].

Having outlined the design procedures for a relatively simple PI-based formation control system we can comment on some of its limitations: the designed system only considers formation in horizontal plane; the PI control is limited to predetermined gains; for more than two aircraft formations, a new design process is required; and the wake-effects due to formation flight do not explicitly form part of the equations modelling the systems. More complex approaches that overcome these limitations are briefly described in the following section.

4.3 More Complex Approaches

Techniques from different branches of control theory have been proposed to tackle the design of formation flight control system. Section 4.2 detailed an approach broadly classified in the *classical* control theory. Other classes of control theory include behavioural control, adaptive control, optimal control, robust control and more. In this section examples of application of these branches for formation flight is briefly outlined.

Giulietti et al. apply a behavioural approach [49]. They propose that any individual aircraft should maintain its position within the formation geometry with respect to an imaginary point in the formation, called the formation geometry center (FGC), whose dynamics are a function of the positions of all the aircraft. The formation controller is comprised of a trajectory controller which is responsible for the tracking of a prescribed path, and a position controller which allows formation geometry keeping. The FGC will allow the individual aircraft of the formation to sense the movement of other vehicles from the nominal position in the formation. In case of a disturbance, when one aircraft loses its position, the other senses the changes, and deviates from the prescribed trajectory momentarily, then manoeuvring to achieve the formation configuration.

Adaptive control can play a crucial role for on-line failure detection, identification and reconfiguration (FDIR). Specifically, the goal is to develop control algorithms that control the formation if one of the aircraft fails to implement control effector to maintain the nominal configuration. Boskovic et al. propose a control system to tackle this problem [50]. They employ the multiple models, switching and tuning (MMST) technique developed in [51]. The rationale for this technique is that the system should be able to operate under a wide operational situations by detecting the specific situation at any given time and responding to it appropriately, for details refer to [51].

McCamish et al. proposed an optimal approach [52]. The optimal approach allows finding the control and state law of the system to achieve an optimal performance, in this case formation maintenance and minimisation of energy requirements of the trailing aircraft in the events of arbitrary formation manoeuvres and the presence of full system nonlinearities.

More recent investigations have proposed robust control systems that incorporate algorithms to compute the geometry separation required to achieve the maximum drag savings during the flight. As previously reported, formation flight benefits reduce rapidly when lateral spacings diverges from the 'sweet spot'. This spot is subject to change due to atmospheric conditions and the constantly changing nature of the wake vortex. [53,54] are two of the papers that propose computation of the separation requirement for maximum benefits during flight and controlling the aircraft in formation appropriately.

[††]Although an attempt was made at a Simulink simulation with the above designs and derived gains values from the papers, time constraint did not allow development of equations of motion for the lead aircraft, V_L and ψ_L which are the disturbance signals for the purposes of this model.

5 Formation Configurations: An Application of the Theory

In this section we investigate induced drag reduction in formation flight by considering a number of formation geometries, using the theory discussed in Section 2.1.

5.1 Motivation

Discussions of various aerodynamics analyses in Section 2 have made it clear that induced drag benefits in formation flight is strongly dependent on the number of aircraft and the aircraft positions relative to each other. For instance, for maximum induced drag savings, low lateral spacings are required. But the induced drag savings can be measured not only in terms of the *total* induced drag reduction due to the formation, but also the effects on *individual* aircraft within the formation. A natural question to ask is: how is the induced drag savings distributed between the aircraft in the formation? With the relatively simple equations shown in Section 2.1, we attempt to answer this question by considering a number of geometries.

5.2 Simplifications

In order to simplify the analysis, we only consider formation of aircraft in the same horizontal plane, i.e. no spacing in the z-direction. This means that from the Biot-Savart law, the vortex strength can be assumed to be constant for all the aircraft. We will also assume that the spacing between the aircraft are uniform, and all the aircraft in the formation have the same wing span. Of course, other assumptions and simplifications from Section 2.1 still apply.

5.3 Governing Equations

For simplicity, we start with computing the velocity induced by a vortex segment of strength Γ, at any point P, shown in Figure 8.

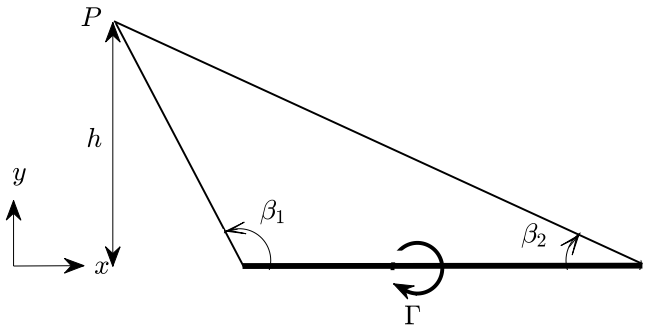

Figure 8: Induced velocity due to a vortex segment.

From Biot-Savart law, the velocity is given as follows

$$\begin{aligned}
\mathbf{v}_P &= \int_0^L \frac{\Gamma}{4\pi}\frac{d\mathbf{l}\times\mathbf{r}}{r^3} \\
&= \int_{\beta_1}^{\pi-\beta_2} \frac{\Gamma}{4\pi}\frac{1}{r^3}\frac{h^2}{\sin^2\theta}d\theta\hat{\mathbf{k}} \\
&= \int_{\beta_1}^{\pi-\beta_2} \frac{\Gamma}{4\pi h}\sin(\theta)d\theta\hat{\mathbf{k}} \\
&= \frac{\Gamma}{4\pi h}\left(-\cos(\pi-\beta_2)+\cos(\beta_1)\right)\hat{\mathbf{k}} \\
&= \frac{\Gamma}{4\pi h}\left(\cos\beta_1+\cos\beta_2\right),
\end{aligned} \tag{20}$$

where we have parameterized the integral by the angle θ, between $\hat{\mathbf{i}}$ and $\mathbf{r}$ such that,

$$\begin{aligned} r &= \frac{h}{\sin\theta} \\ x &= -h\cot\theta \qquad \Rightarrow \quad dx = \frac{hd\theta}{\sin^2\theta} \\ d\mathbf{l}\times\mathbf{r} &= dxr\sin\theta\hat{\mathbf{k}} = \frac{h^2}{\sin^2\theta}d\theta\hat{\mathbf{k}}, \end{aligned}$$

and as x goes from the left edge of the vortex segment to the right edge, θ goes from β_1 to $\pi-\beta_2$.

With the final expression from Eqn. 20 the velocity due to a horseshoe vortex can be calculated in three stages, following the coordinate system defined in Figure 1 with b denoting the wingspan: the induced velocity due to the left trailing vortex ($y=-b/2$), the bound portion ($x=0$), and the right trailing vortex ($y=b/2$). For each we need the distance from the point to the vortex segment h, and the angles β_1 and β_2.

For the left trailing vortex, the distance from our point of interest to this vortex is,

$$h_L = \sqrt{(b/2+y)^2+z^2}.$$

The direction of the velocity induced by this vortex is in the $y-z$ plane and is given by $z/h_L\hat{\mathbf{j}}-(b/2+y)/h_L\hat{\mathbf{k}}$. Since, the vortex is semi-infinite one of the angles is zero and thus has cosine of 1, and the other one has a cosine of $x/\sqrt{h_L^2+x^2}$. Therefore, the velocity induced by the left trailing vortex is

$$\mathbf{v}_L = \frac{\Gamma}{4\pi h_L}\left[\frac{x}{\sqrt{h_L^2+x^2}}+1\right]\left[\frac{z}{h_L}\hat{\mathbf{j}}-\frac{b/2+y}{h_L}\hat{\mathbf{k}}\right].$$

For the induced velocity due to the right trailing vortex, we follow a similar procedure, and thus have

$$\begin{aligned} h_R &= \sqrt{(b/2-y)^2+z^2}, \\ \mathbf{v}_R &= \frac{\Gamma}{4\pi h_R}\left[\frac{x}{\sqrt{h_R^2+x^2}+1}\right]\left[-\frac{z}{h_R}\hat{\mathbf{j}}-\frac{b/2-y}{h_R}\hat{\mathbf{k}}\right]. \end{aligned}$$

Finally, for the bound portion, the distance and angles are,

$$\begin{aligned} h_B &= \sqrt{x^2+z^2}, \\ \cos\beta_{B,1} &= \frac{b/2-y}{\sqrt{h_B^2+(b/2-y)^2}}, \\ \cos\beta_{B,2} &= \frac{b/2+y}{\sqrt{h_B^2+(b/2+y)^2}}, \end{aligned}$$

and thus the induced velocity in the $x-z$ plane with the direction $z/h_B\hat{\mathbf{i}}-x/h_B\hat{\mathbf{k}}$ is given by,

$$\mathbf{v}_B = \frac{\Gamma}{4\pi h_B}\left[\cos\beta_{B,1}+\cos\beta_{b,2}\right]\left[z/h_B\hat{\mathbf{i}}-x/h_B\hat{\mathbf{k}}\right].$$

Therefore, the total induce velocity due to a single horseshoe vortex at any point is,

$$\mathbf{v}_{\text{induced}} = \mathbf{v}_L+\mathbf{v}_R+\mathbf{v}_B, \tag{21}$$

and the total induced velocity due to the formation is,

$$\mathbf{v}_{\text{induced}}^{\text{formation}} = \sum_{i=1}^{N}\mathbf{v}_{\text{induced,i}}. \tag{22}$$

5.4 Geometries

The various configurations to be considered in this study are shown in Figure 9 for a representative number of aircraft in each case.

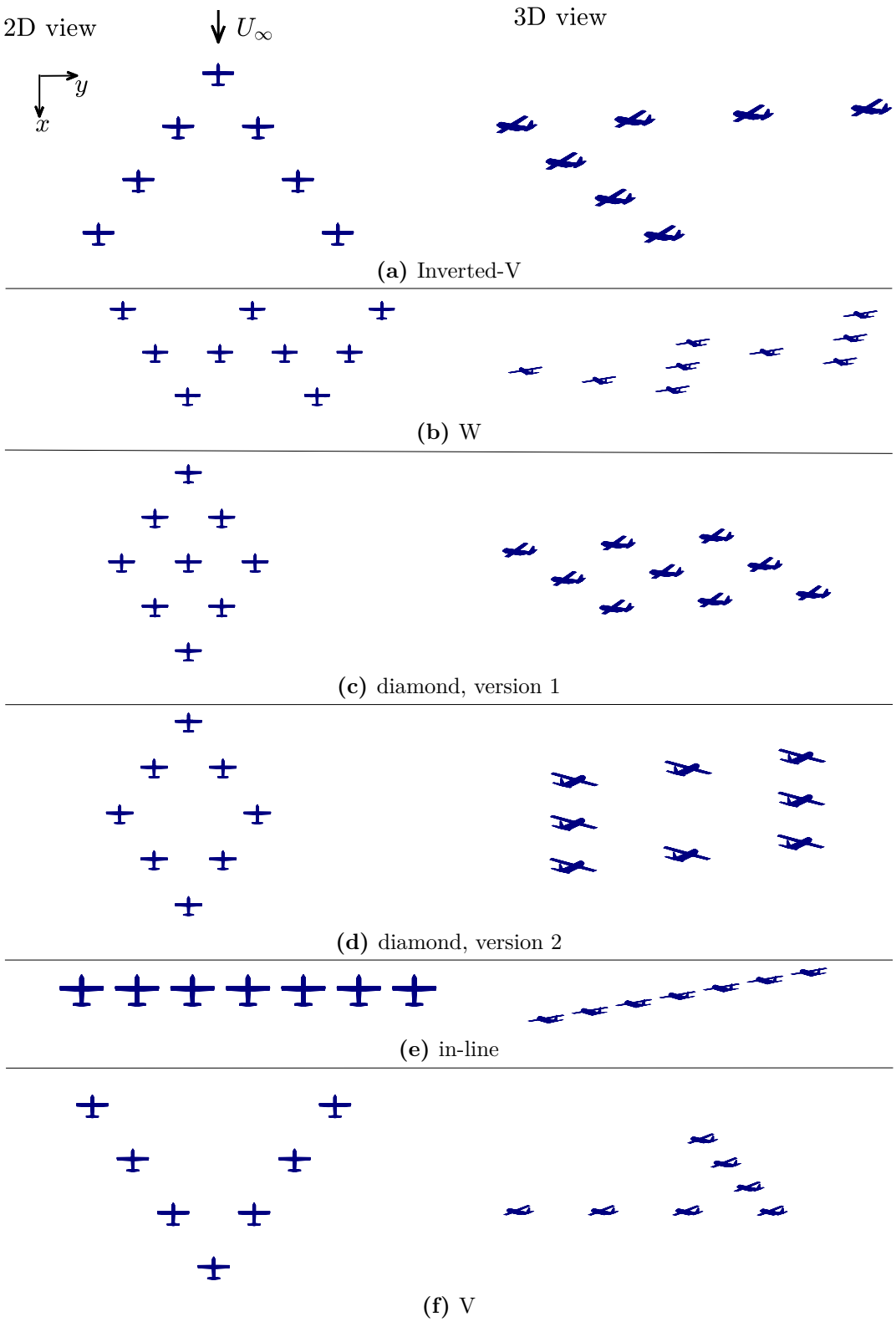

(a) Inverted-V

(b) W

(c) diamond, version 1

(d) diamond, version 2

(e) in-line

(f) V

Figure 9: The six formation configurations to be simulated for this study.

5.5 MATLAB Implementation

Figure 10 outlines the simulation procedure followed with description of each step.

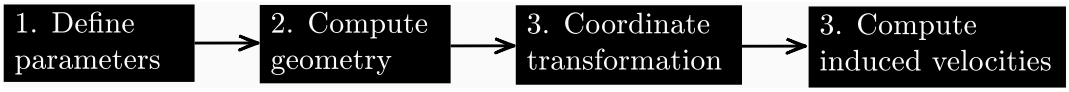

Figure 10: Simulation process flow diagram

1. Define parameters: the aircraft and formation geometry characteristics are specified. These will form the inputs for variously functions for the simulation. Specifically,
   (a) individual aircraft parameters: wing span, wing area, estimated weight, cruise altitude air density and velocity
   (b) formation geometry: number of aircraft in formation, and longitudinal and lateral spacings between aircraft
2. Compute geometry: The aircraft positions are computed based on the following inputs: spacings, number of aircraft, and geometry type. Available geometries are those shown in Figure 9. The outputs are coordinates of the centre of each wing in formation.
3. Coordinate transformation: the global coordinates from step 2 are transformed to local coordinates for each aircraft. Specifically, each local coordinate has the aircraft under consideration at the origin, with positions of the other wings defined relative to this aircraft at the origin. This is a crucial process as it will allow computing the induced velocities of all the aircraft at the centre of each wing.
4. Compute induced velocities: The induced velocities on each aircraft is computed using the equations outlined in Section 5.3. Specifically, loop over each set of local coordinates and compute:
   (a) the velocity at the wing centre of the aircraft at the origin due to its own trailing vortices,
   (b) the velocity the aircraft at the origin induces on all the other aircraft,
   (c) total induced drag for the formation.

Finally, the results can be post-processed further, such as: plotting the various quantities for comparison of the different formation configurations.

5.6 Verification

In order to verify that the MATLAB implementation is correct, we calculate the downwash for a two aircraft formation using the codes described in Section 5.5 and using the following equations derived manually from the governing equations[‡‡], for the geometry shown in Figure 11.

$$\begin{aligned} w_1(0) = &-\frac{\Gamma}{\pi b} + \frac{\Gamma}{4\pi b(\beta+1/2)}\left(1-\frac{\gamma b}{r_1}\right) - \frac{\Gamma}{4\pi b(\beta+3/2)}\left(1-\frac{\gamma b}{r_2}\right) \\ &+ \frac{\Gamma}{4\pi\gamma b}\left(\frac{-(\beta+1/2)b}{r_1} + \frac{(\beta+3/2)b}{r_2}\right), \end{aligned} \tag{23}$$

$$\begin{aligned} w_2(0) = &-\frac{\Gamma}{\pi b} + \frac{\Gamma}{4\pi b(\beta+1/2)}\left(1+\frac{\gamma b}{r_1}\right) - \frac{\Gamma}{4\pi b(\beta+3/2)}\left(1+\frac{\gamma b}{r_2}\right) \\ &- \frac{\Gamma}{4\pi\gamma b}\left(\frac{-(\beta+1/2)b}{r_1} + \frac{(\beta+3/2)b}{r_2}\right), \end{aligned} \tag{24}$$

[‡‡]From *AEROSP 325: Aerodynamics*, course notes by Prof. K. Fidkowski.

where $w_1(0)$ and $w_2(0)$ are the downwash ($\hat{\mathbf{k}}$ component of the induced velocity) for each aircraft,

$$r_1 = b\sqrt{(\beta + 1/2)^2 + \gamma^2} \qquad \text{and} \qquad r_2 = b\sqrt{(\beta + 3/2)^2 + \gamma^2}). \tag{25}$$

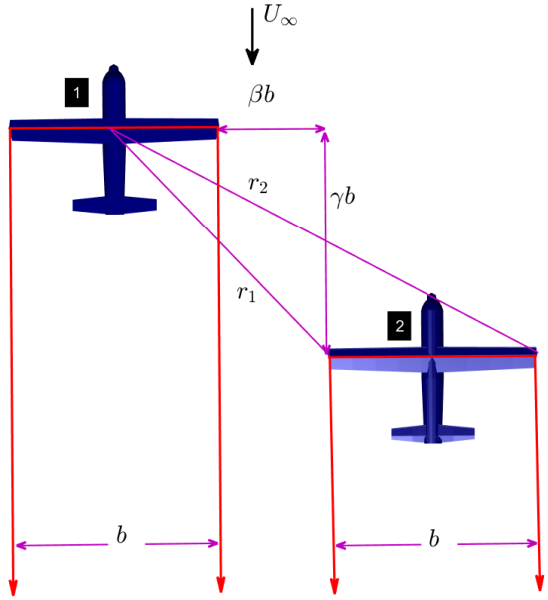

Figure 11: Geometry used for code verification.

With the parameters, $b = \Gamma = 1$ and $\beta = \gamma = 0.5$, the results from the simulation and evaluation of Eqns. 23, 24 are: $w_1(0) = -0.2924$ and $w_2(0) = -0.2646$. Thus, verifying that the codes perform the simulation correctly.

5.7 Results

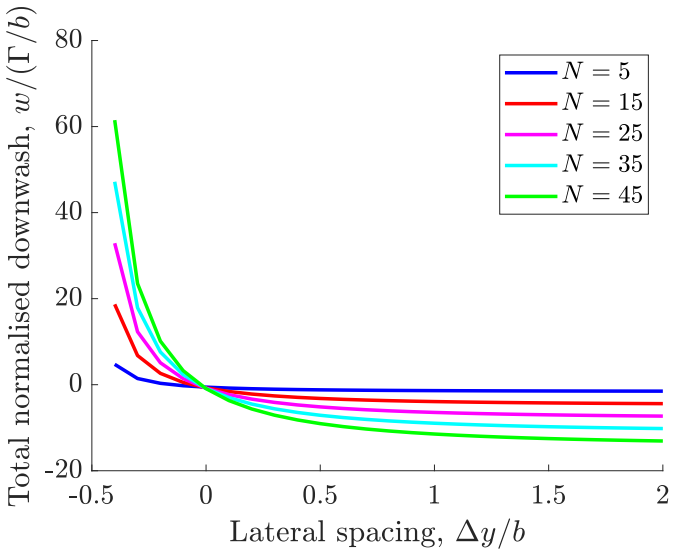

Figure 12: The total downwash due to formation for various lateral spacings, a longitudinal spacing of 10 wingspans, and different number of aircraft in the formation.

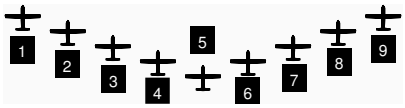

(a) Horizontal axis label

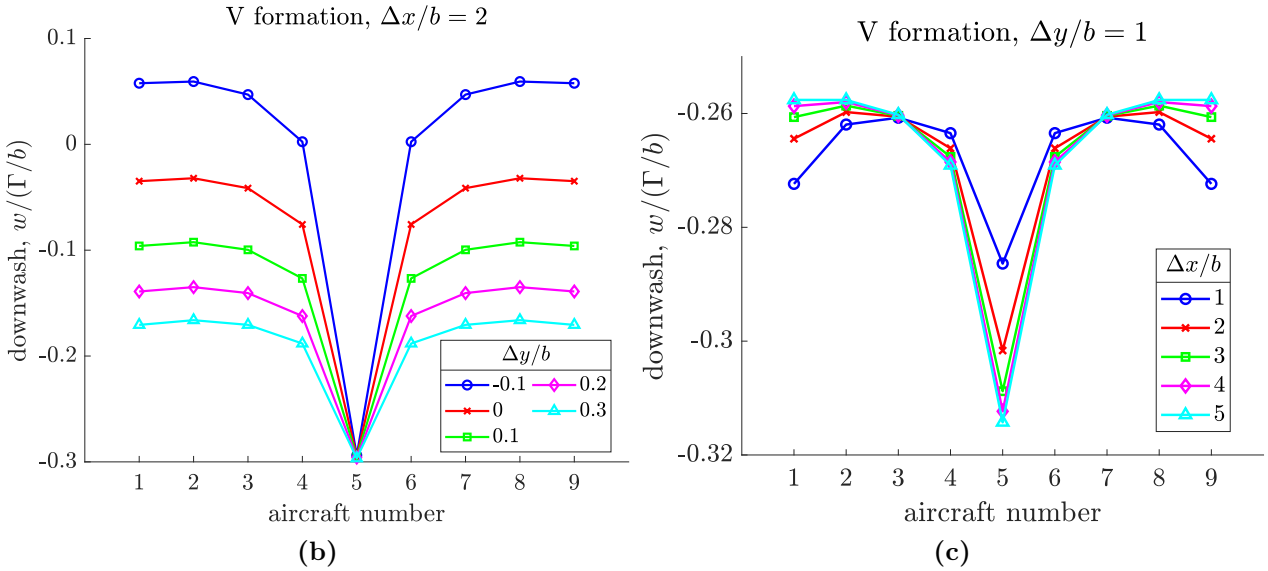

(b) **(c)**

Figure 13: Downwash on individual aircraft with (b) constant longitudinal spacing, (c) constant lateral spacing, with nine aircraft in formation.

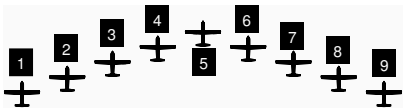

(a) Horizontal axis label

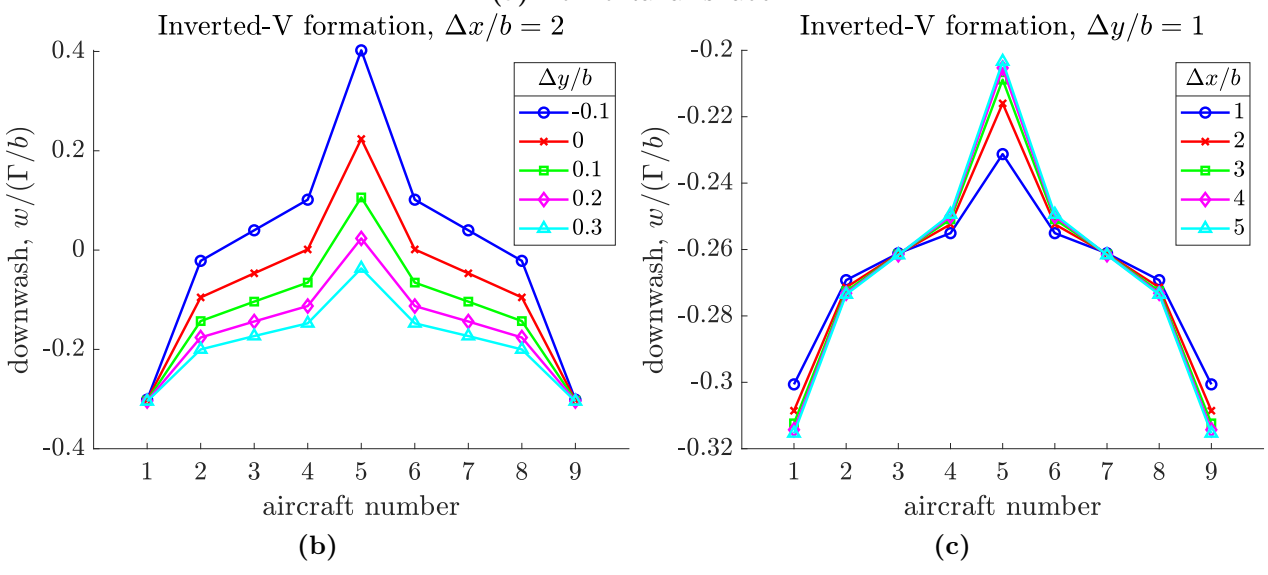

(b) **(c)**

Figure 14: Downwash on individual aircraft with (b) constant longitudinal spacing, (c) constant lateral spacing, for nine aircraft in formation.

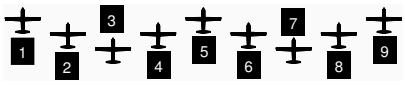

(a) Horizontal axis label

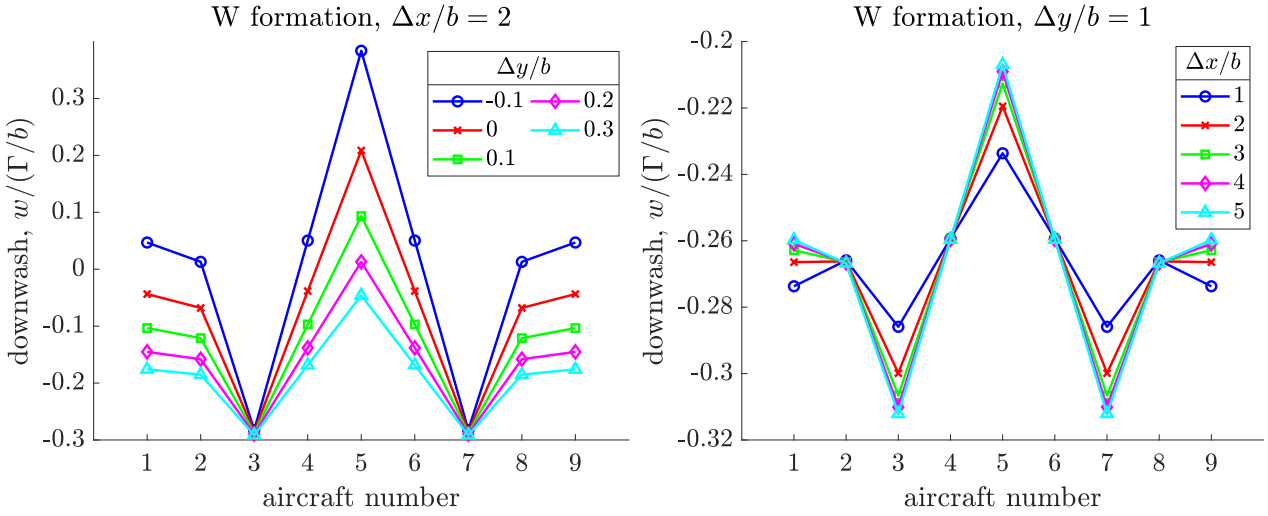

(b) **(c)**

Figure 15: Downwash on individual aircraft with (b) constant longitudinal spacing, (c) constant lateral spacing, for nine aircraft in formation.

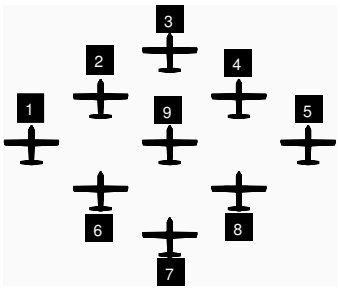

(a) Horizontal axis label

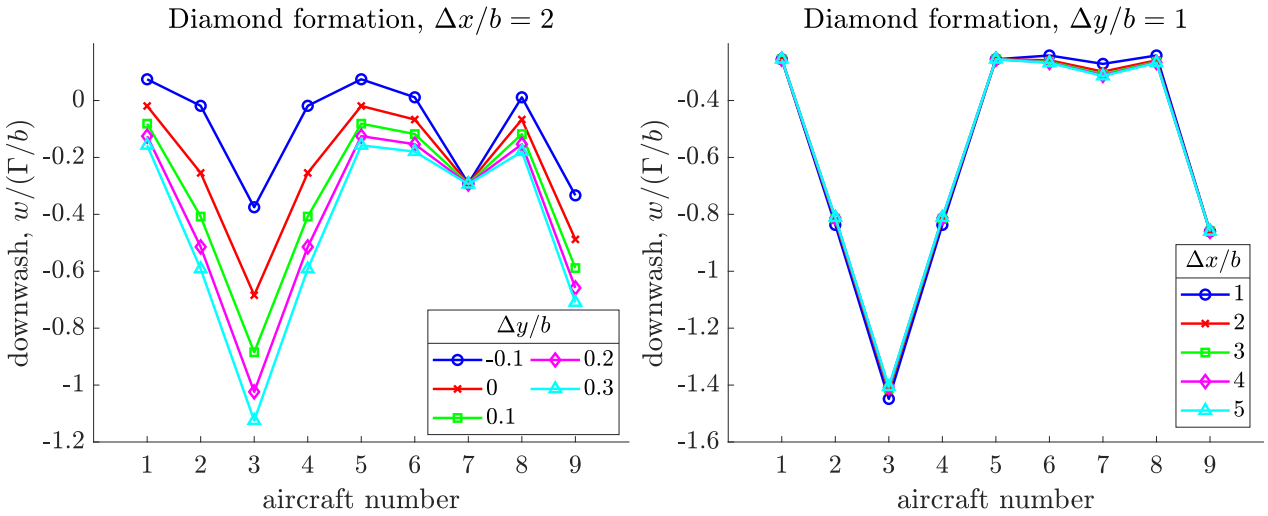

(b) **(c)**

Figure 16: Downwash on individual aircraft with (b) constant longitudinal spacing, (c) constant lateral spacing, for nine aircraft in formation.

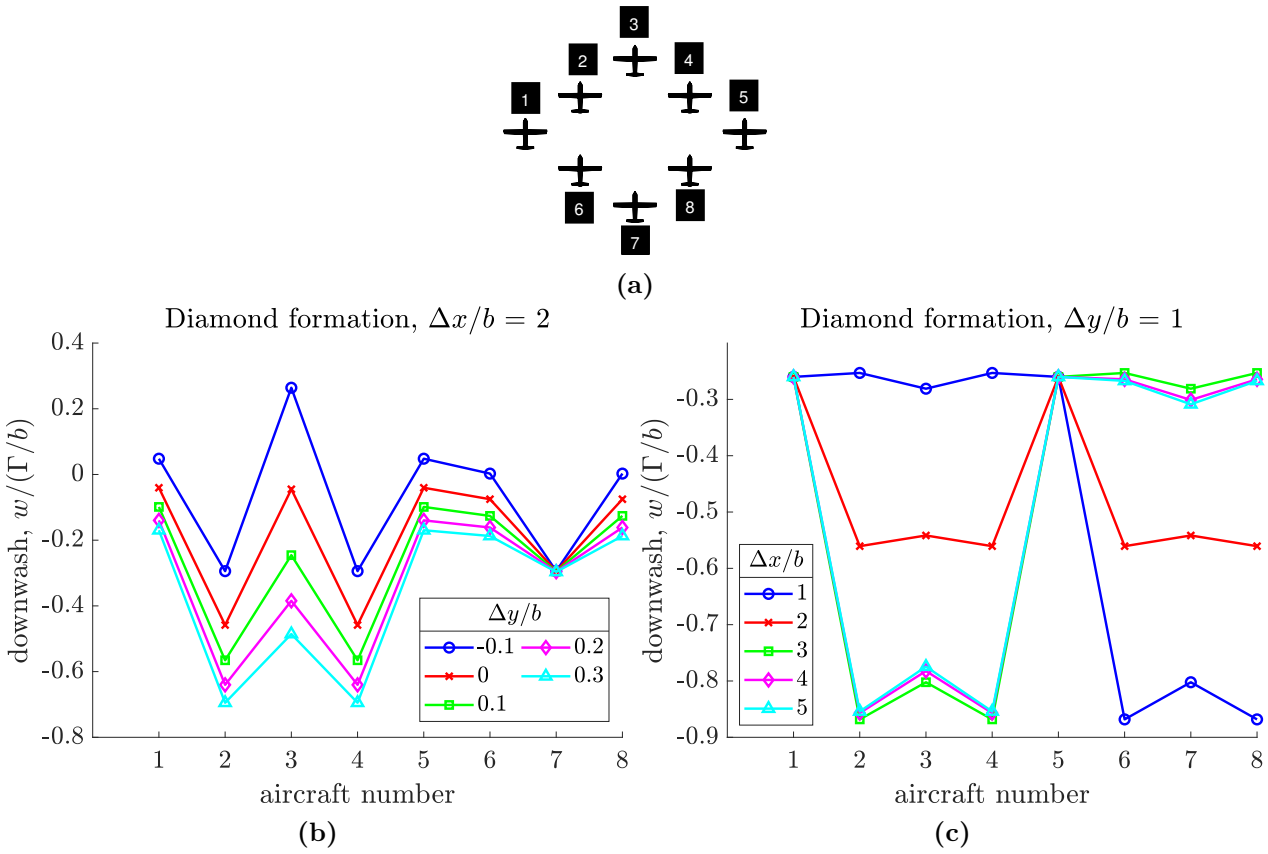

Figure 17: Downwash on individual aircraft with (b) constant longitudinal spacing, (c) constant lateral spacing, for eight aircraft in formation. Different from Figure 16, as the aircraft at the centre is removed.

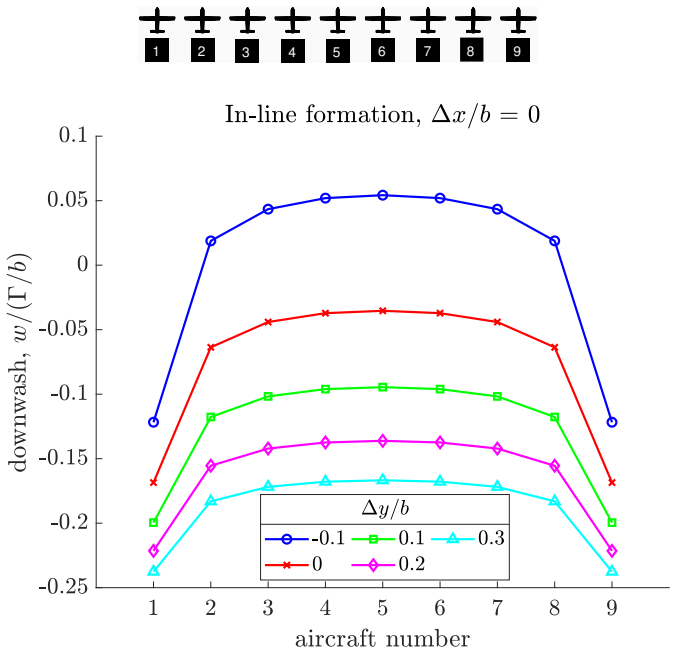

Figure 18: Downwash on individual aircraft with varying lateral spacings.

5.8 Discussion

The results for the induced velocity for the whole formation and individual aircraft within the formation compared against various number of aircraft, and longitudinal and lateral separations between aircraft have been reported in the preceding section. Specifically, the *downwash*, induced velocity in the direction perpendicular to the formation plane (the $-z$ direction in the coordinates defined in Figure 1), are reported since the the component along the axes of the plane are zero.

From the generalised Kutta-Joukowski, Eqn. 1, the lift and induced drag for a single horseshoe vortex wing representation is given as,

$$L = \rho b \Gamma U_\infty \qquad and \qquad D_i = -\rho b \Gamma w(0) \tag{26}$$

where ρ is the air density, b is the wing span, Γ is the vortex strength, U_∞ is the horizontal freestream velocity in the x direction, and $w(0)$ is the downwash at the middle of the bound vortex on the wing. The key information to note is that for constant air density and circulation distribution Γ, the induced drag is directly proportional to the downwash.

Figure 12 shows the total formation downwash as a function of lateral spacing and constant longitudinal spacing of ten wingspans, for various number of aircraft within a V-formation. First point to note is that for the same variation of number of aircraft and lateral spacing, the results will not change even if the longitudinal spacing is varied. This is explained by Munk's stagger theorem which states that the induced drag, and as consequence the induced velocity, of a system is independent of the longitudinal spacing of the individual components of the system so long as the circulation distributions on the elements are left unchanged, for proof refer to [55]. Secondly, the figure shows that with overlapping wings, up to 50% of the span, the entire formation experiences upwash, hence maximum induced drag savings. As the lateral separation increases, the formation effects on the downwashes diminish rapidly. For small wing overlaps, the benefits are marginal for when the number of aircraft in formation is increased.

Figure 13 through 18 show the downwash distribution for various formation configurations comprised of nine aircraft, as a function of lateral and longitudinal separations.

First, we compare the V and inverted-V formations. In both cases the aircraft at the apex is most sensitive to the longitudinal spacing, with the magnitude of the downwash increasing as the longitudinal spacing increases. In terms of the lateral spacing, the downwash for the aircraft at the apex of the V-formation is insensitive to the lateral spacing, and achieves the maximum downwash as it benefits from the vortices of all the leading aircraft. On the other hand, for the inverted-V formation the downwash for the aircraft at the apex changes with changing lateral separation, however the downwash remains insensitive for the aircraft at the edges. As expected, the magnitude of the downwash is highly dependent on the lateral spacing, increasing with higher lateral separations.

For the W-formation, in terms of lateral spacing, the aircraft at the centre, (aircraft 5 in Figure 15a) is most sensitive while the trailing apex aircraft remain insensitive. The aircraft that have leading and trailing neighbours on both sides have similar downwashes from symmetry. These aircraft remain insensitive to longitudinal spacings for a given lateral spacing.

For the diamond formations the results show that for the case where an aircraft is placed at the origin of the formation the longitudinal spacings do not affect the downwash distribution much, and the aircraft at lower boundaries of the diamond have similar downwashes. But for case where the aircraft from the origin is excluded, longitudinal spacings does effect the distribution. In both cases, the aircraft at the lower apex remains insensitive to changes in laterals spacings, while the magnitude of the downwash increases with increasing lateral spacing.

For the in-line formation, the downwash reduces the further away an aircraft is from the centre of the formation, as expected. Also, the distribution is fairly sensitive to the lateral spacing.

6 Conclusions and Future Work

The literature review has shown that critical aspects of formation flight - aerodynamics and controls - have been investigated relatively extensively. Theoretical aerodynamic modelling and experimental studies show considerable benefit from flying in formation. The simplest aerodynamic model available is a horseshoe model which neglects wake roll-up, but very simple to apply. A common higher-fidelity approach is the vortex lattice method which can account for wake roll up effects. CFD analysis of a two aircraft formation in transonic regime has shown that some benefits are lost when compressibility effects are taken in to account.

Analyses have also shown that longitudinal separations between aircraft has little effect on the savings for the whole formation. Thus extended formation flight - minimum spanwise separation of five wingspans - is particularly useful in terms of safety for commercial application. Other aspects for commercial flights that requires further exploration include: route optimisation; ride quality analysis; etc.

Various control systems have been proposed based on both classical and modern control theory, although for extended formation flight further investigations in sensor technologies are recommended.

The following topics can be explored in future studies, within the scope of a similar project this report has been produced for, not general investigations of formation flight:

- A number of simplifications were made for the single horseshoe vortex aircraft model used in this project, outlined in Section 5.2, future projects could improve these by considering:
  - vertical spacing between aircraft (z-direction in Figure 1) to define the formation geometry,
  - heterogeneous aircraft within the formation, i.e. aircraft with different spans,
  - non-symmetric formations with non-uniform spacings between each aircraft,
  - more appropriate definitions of metrics determining formation benefits (e.g. percent fuel savings, drag coefficients), etc.
- Use a vortex-sheet wing representation for simulations, by either writing own codes, or using AVL.
- Apply optimisation techniques to find optimum formation configurations for more conclusive results than found in Section 5.
- Design control laws and perform simulations based on model discussed in Section 4.2.
- Perform literature search of other aspects of the commercial application of formation flight: route optimisation; sensing technologies, etc.

7 Appendices

Listing 1: MATLAB function to compute formation configurations.

```
1  function pos = geometry(dx,dy,N,b,type, p)
2  % PURPOSE: this function computes the formation configuration
3  %  INPUTS:
4  %       dx, dy : longitudinal and lateral spacing between bodies
5  %       N      : number of bodies
6  %       b      : span
7  %       type   : string to specify geometry to be computed
8  %       p      : scalar, 1 or 0, to determine if geometry should be plotted
9  %  OUTPUTS:
10 %       pos    : an (N x 3) vector [x,y,z]
11 %       figure : formation geometry
12 %  Additional function:
13 %       c130k  : used to plot formation geometry
14 %                available @ https://tinyurl.com/y5kjdoze [Mathworks.com]
15
```

```
pos = zeros(N,3);  % initialise

% V, INVERTED-V, STRAIGHT LINE (HORIZONTAL AND VERTICAL) FORMATIONS
geom = {'V','iV','h','v'};
tf = strcmp(type,geom);
if any(tf == 1)
    if tf(1) == 1, x1 = 1; x2 = x1; end                % V-formation
    if tf(2) == 1, x1 = -1; x2 = x1; end               % inverted-V formation
    if tf(3) == 1, x1 = 1; x2 = x1; dx = 0; end        % horizontal
    if tf(4) == 1, x1 = -1; x2 = 1; dy = 0; b=0; end % vertical
    nm = (N+1)/2;
    for n = 1:nm-1
        pos(nm+n,:) = [x1*n*dx, n*(dy+b), 0]; % right-leg of formation
        pos(nm-n,:) = [x2*n*dx, -n*(dy+b), 0]; % left-leg
    end
end

% W FORMATION
if type == 'W'
    nm = (N+1)/2;
    % leading bodies (left to right)
    pos(1,:) = [0,-(nm-1)*(dy+b), 0];
    pos(nm,:) = [0,0,0];
    pos(N,:) = [0,(nm-1)*(dy+b), 0];
    % trailing bodies (left to right)
    pos(nm+(nm-1)/2,:)= [-0.5*(N-nm)*dx, 0.5*(N-nm)*(dy+b), 0];
    pos(nm-(nm-1)/2,:) = [-0.5*(N-nm)*dx, -0.5*(N-nm)*(dy+b),0];
    % the bodies in between
    x = N-nm-2;
    for n = 1:(N-nm)/2 -1
        pos(nm+n,:) = [-n*dx, n*(dy+b),0];
        pos(nm-n,:) = [-n*dx, -n*(dy+b),0];
        pos(nm+n+x,:) = [-n*dx, (n+x)*(dy+b),0];
        pos(nm-n-x,:) = [-n*dx, -(n+x)*(dy +b),0];
        x = x - 2;
    end
end

% DIAMOND FORMATION
if type == 'D'
    % place an body at origin if N is odd
    if mod(N,2) == 0, M = N; else M = N - 1; end
    nE = M/2 + 1; nW = 1; nN = M/4 + 1; nS = nE + M/4;
    d = nE - nN; % distance between ac in north and east
    pos(nE,:) = [0,d*(dy+b),0];      % east
    pos(nW,:) = [0, -d*(dy+b), 0]; % west
    pos(nN,:) = [0.25*M*dx, 0, 0];  % north
    pos(nS,:) = [-0.25*M*dx, 0, 0]; % south
    for n = 1:d-1
        pos(nN+n,:) = [(d-n)*dx, n*(dy+b), 0];
        pos(nS+n,:) = [-(d-n)*dx, n*(dy+b), 0];
        pos(nW+n,:) = [(d-n)*dx, -n*(dy+b), 0];
        pos(nW+M/2+n, :) = [-(d-n)*dx, -n*(dy+b), 0];
    end
end

% PLOT FORMATION IF ON
if p == 0, return, end
if p == 1
    figure
    for i = 1:N
        hold on
        x = pos(i,2); y = pos(i,1); z = pos(i,3);
        c130k(x,y,z,'scale', 0.03);
        hold off
    end
    xlabel('Lateral, y'); ylabel('Longitudinal, x');
    grid on; axis equal;
end
```

Listing 2: MATLAB function to compute the induced velocity.

```
function v = vhorse(pos)
% The inputs x,y,z are assumed nondimensionalized by b
% The output v (velocity) is nondimensionalized by Gamma/b
x = pos(1); y = pos(2); z = pos(3);
% left trailing vortex
hL = sqrt((0.5+y)^2+z^2);
vL = 1/(4*pi*hL)*(x/sqrt(hL^2+x^2)+1)*[0,z/hL, -(0.5+y)/hL];

% right trailing vortex
hR = sqrt((0.5-y)^2+z^2);
vR = 1/(4*pi*hR)*(x/sqrt(hR^2+x^2)+1)*[0,-z/hR, -(0.5-y)/hR];

% bound portion
hB = sqrt(x^2+z^2);
cosB1 = (0.5-y)/sqrt(hB^2 + (0.5-y)^2);
cosB2 = (0.5+y)/sqrt(hB^2 + (0.5+y)^2);
vB = 1/(4*pi*hB)*(cosB1+cosB2)*[z/hB, 0, -x/hB];

% induced velocity
v = [vL; vB; vR];

% Identify NaN component
TF = isnan(v(2,:));
if TF == ones(1,3), v(2,:) = []; end

v = sum(v);
```

Listing 3: MATLAB function to perform the simulations by using the functions in Listings 1 and 2.

```
function [vitotal, vi] = horseshoemodel(glblpos, b)
% Function to compute induced velocities given aircraft formation geometery
% INPUT:
%   glbl pos: [N x 3] matrix of aircraft positions in formation (assume
%   positions arranged left to right)
%   b       : wing span
% OUTPUTS:
%   vitotal :    total induced velocity of the formation
%   vi      :    vector of induced velocities on each aircraft
% Built-in function used:
%   global2localcoord

N = size(glblpos,1);        % number of aircraft

% switch to local coordinates for each aircraft
for i=1:N
    for j = 1:N
        lclCoordtemp(j,:) = global2localcoord(glblpos(j,:)', 'rr', glblpos(i,:)');
    end
    lclCoord{i} = lclCoordtemp;
end

vi_formation = zeros(N,3);        % initialise
% compute induced velocity for the formation
for i = 1:N
    lcl = lclCoord{1,i};
    for j = 1:N
        vi_formation(j,:) = vhorse(lcl(j,:)/b) + vi_formation(j,:);
    end
end
vi = vi_formation(:,3);        % induced velocity on each aircraft
vitotal = sum(vi); % induced velocity for the formation
```

Acknowledgements

I would like to thank Prof. Fidkowski for giving me the opportunity for this directed-study project. I have learnt a lot from our weekly update meetings through out this project, and from his other classes.

Also thanks to Prof. Gorodetsky for allowing me to look in to the control aspects of formation flight and helpful feedback.

Image credit: the C-130 model used for various images through out this report are based on adapted codes found on MathWorks website, written by Chad Greene, codes available here: `https://tinyurl.com/y5kjdoze`.

References

[1] D. Hummel, "Aerodynamic aspects of formation flight in birds," *Journal of theoretical Biology*, vol. 104, no. 3, pp. 321–347, 1983.

[2] J. Brisswalter and C. Hausswirth, "Consequences of drafting on human locomotion: benefits on sports performance," *International Journal of Sports Physiology and Performance*, vol. 3, no. 1, pp. 3–15, 2008.

[3] A. Ning, T. C. Flanzer, and I. M. Kroo, "Aerodynamic performance of extended formation flight," *Journal of aircraft*, vol. 48, no. 3, pp. 855–865, 2011.

[4] Y. Liu and E. Stumpf, "Estimation of vehicle-level fuel burn benefits of aircraft formation flight," *Journal of Aircraft*, vol. 55, no. 2, pp. 853–861, 2017.

[5] F. H. Heppner, "Avian flight formations," *Bird-Banding*, vol. 45, no. 2, pp. 160–169, 1974.

[6] P. Lissaman and C. A. Shollenberger, "Formation flight of birds," *Science*, vol. 168, no. 3934, pp. 1003–1005, 1970.

[7] J. R. Speakman and D. Banks, "The function of flight formations in greylag geese anser anser; energy saving or orientation?," *Ibis*, vol. 140, no. 2, pp. 280–287, 1998.

[8] J. D. Anderson Jr, *Fundamentals of aerodynamics*. Tata McGraw-Hill Education, 2010.

[9] C. Wieselsberger, "Beitrag zur erklarung des winkelfluges eineger zugvogel, z. flugtechnik ," *Motorluftschiffahrt*, vol. 5, pp. 225–229, 1914.

[10] A. Gopalarathnam, "Aerodynamic benefit of aircraft formation flight," *Encyclopedia of Aerospace Engineering*, 2010.

[11] D. Hummel, "Formation flight as an energy-saving mechanism," *Israel Journal of Ecology and Evolution*, vol. 41, no. 3, pp. 261–278, 1995.

[12] P. Lissaman, "Simplified analytical methods for formation flight or ground effect," in *43rd AIAA Aerospace Sciences Meeting and Exhibit*, p. 851, 2005.

[13] J. D. Haffner, "A flapping wing model for avian formation flight," 1977.

[14] W. Blake and D. Multhopp, "Design, performance and modeling considerations for close formation flight," in *23Rd atmospheric flight mechanics conference*, p. 4343, 1998.

[15] A. E. Albright, C. J. Dixon, and M. C. Hegedus, *Modification and validation of conceptual design aerodynamic prediction method HASC95 with VTXCHN*, vol. 4712. National Aeronautics and Space Administration, 1996.

[16] M. Drela and H. Youngren, "Avl," *URL http://web. mit. edu/drela/Public/web/avl/. Diakses*, vol. 14, 2014.

[17] D. Hummel, "Recent aerodynamic contributions to problems of bird flight," in *ICAS Proceedings, 11th Congress of the International Council of the Aeronautical Sciences*, pp. 10–16, 1978.

[18] J. R. Spreiter, "The rolling up of the trailing vortex sheet and its effect on the downwash behind wings," *Journal of the Aeronautical Sciences*, vol. 18, no. 1, pp. 21–32, 1951.

[19] B. Maskew, "Formation flying benefits based on vortex lattice calculations," 1974.

[20] T. Sarpkaya, "Computational methods with vortices: the 1988 freeman scholar lecture," *Journal of Fluids Engineering*, vol. 111, no. 1, pp. 5–52, 1989.

[21] R. Krasny, "Computation of vortex sheet roll-up in the trefftz plane," *Journal of Fluid mechanics*, vol. 184, pp. 123–155, 1987.

[22] H. W. M. Hoeijmakers and W. Vaatstra, "A higher order panel method applied to vortex sheet roll-up," *AIAA Journal*, vol. 21, no. 4, pp. 516–523, 1983.

[23] G. R. Baker, "The cloud in cell technique applied to the roll up of vortex sheets," *Journal of Computational Physics*, vol. 31, no. 1, pp. 76–95, 1979.

[24] A. J. Chorin and P. S. Bernard, "Discretization of a vortex sheet, with an example of roll-up," *Journal of Computational Physics*, vol. 13, no. 3, pp. 423–429, 1973.

[25] E. Murman and P. Stremel, "A vortex wake capturing method for potential flow calculations," in *3rd Joint Thermophysics, Fluids, Plasma and Heat Transfer Conference*, p. 947, 1982.

[26] G. Bramesfeld, "A higher order vortex-lattice method with a force-free wake," 2006.

[27] G. Bramesfeld, M. Maughmer, and K.-H. Horstmann, "A free-wake, lifting-surface model using distributed vorticity elements," in *22nd Applied Aerodynamics Conference and Exhibit*, p. 5075, 2004.

[28] G. Bramesfeld and M. Maughmer, "The effects on formation-flight aerodynamics due to wake rollup," in *45th AIAA Aerospace Sciences Meeting and Exhibit*, p. 729, 2008.

[29] L. Veldhuis, M. Voskuijl, and B. Fransen, "Formation flight-fine-tuning of theoretical performance prediction," in *51st AIAA Aerospace Sciences Meeting including the New Horizons Forum and Aerospace Exposition*, p. 961, 2013.

[30] D. Singh, A. Antoniadis, P. Tsoutsanis, H.-S. Shin, A. Tsourdos, S. Mathekga, and K. Jenkins, "A multi-fidelity approach for aerodynamic performance computations of formation flight," *Aerospace*, vol. 5, no. 2, p. 66, 2018.

[31] A. Inasawa, F. Mori, and M. Asai, "Detailed observations of interactions of wingtip vortices in close-formation flight," *Journal of Aircraft*, vol. 49, no. 1, p. 206 to 213, 2012.

[32] J. P. Slotnick, "Computational aerodynamic analysis for the formation flight for aerodynamic benefit program," *52nd Aerospace Sciences Meeting*, 2014.

[33] S. Ning and I. Kroo, "Compressibility effects of extended formation flight," *29th AIAA Applied Aerodynamics Conference*, 2011.

[34] J. E. Kless, M. J. Aftosmis, S. A. Ning, and M. Nemec, "Inviscid analysis of extended-formation flight," *AIAA Journal*, vol. 51, no. 7, p. 1703 to 1715, 2013.

[35] M. Beukenberg and D. Hummel, "Aerodynamics, performance and control of airplanes in formation flight," in *ICAS, Congress, 17 th, Stockholm, Sweden, Proceedings.*, vol. 2, pp. 1777–1794, 1990.

[36] B. Cobleigh, "Capabilities and future applications of the nasa autonomous formation flight (aff) aircraft," in *1st UAV Conference*, p. 3443, 2002.

[37] R. Ray, B. Cobleigh, M. Vachon, and C. St. John, "Flight test techniques used to evaluate performance benefits during formation flight," in *AIAA Atmospheric Flight Mechanics Conference and Exhibit*, p. 4492, 2002.

[38] M. J. Vachon, R. Ray, K. Walsh, and K. Ennix, "F/a-18 aircraft performance benefits measured during the autonomous formation flight project," in *AIAA atmospheric flight mechanics conference and exhibit*, p. 4491, 2002.

[39] E. Wagner, D. Jacques, W. Blake, and M. Pachter, "Flight test results of close formation flight for fuel savings," in *AIAA Atmospheric Flight Mechanics Conference and Exhibit*, p. 4490, 2002.

[40] J. Pahle, D. Berger, M. Venti, C. Duggan, J. Faber, and K. Cardinal, "An initial flight investigation of formation flight for drag reduction on the c-17 aircraft," in *AIAA atmospheric flight mechanics conference*, p. 4802, 2012.

[41] C. E. Hanson, J. Pahle, J. R. Reynolds, and S. Andrade, "Experimental measurements of fuel savings during aircraft wake surfing," in *2018 Atmospheric Flight Mechanics Conference*, p. 3560, 2018.

[42] W. Blake and D. R. Gingras, "Comparison of predicted and measured formation flight interference effects," *Journal of Aircraft*, vol. 41, no. 2, pp. 201–207, 2004.

[43] I. Korkischko and R. Konrath, "Formation flight of low-aspect-ratio wings at low reynolds number," *Journal of Aircraft*, vol. 54, no. 3, pp. 1025–1034, 2016.

[44] A. Redeker, "Computer aided flight testing of a digital autopilot on board a research aircraft,"

[45] P. R. Rohs, "A fully coupled, automated formation control system for dissimilar aircraft in maneuvering formation flight," tech. rep., Air Force Institute of Technology, Wright-Patterson, AFB OH, School of Engineering, 1991.

[46] L. Buzogany, M. Pachter, and J. D'azzo, "Automated control of aircraft in formation flight," in *Guidance, Navigation and Control Conference*, p. 3852, 1993.

[47] J. L. Dargan, "Proportional plus integral control of aircraft for automated maneuvering formation flight," tech. rep., Air Force Institute of Technology Wright-Patterson, AFB OH, School of Engineering, 1991.

[48] L. E. Buzogany, "Automated control of aircraft in formation flight," tech. rep., Air Force Inst of Tech Wright-Patterson AFB OH School of Engineering, 1992.

[49] F. Giulietti, M. Innocenti, and L. Pollini, "Formation flight control-a behavioral approach," in *AIAA Guidance, Navigation, and Control Conference and Exhibit*, p. 4239, 2001.

[50] J. D. Boskovic and R. K. Mehra, "An adaptive reconfigurable formation flight control design," in *Proceedings of the 2003 American Control Conference, 2003.*, vol. 1, pp. 284–289, IEEE, 2003.

[51] K. S. Narendra and J. Balakrishnan, "Adaptive control using multiple models," *IEEE transactions on automatic control*, vol. 42, no. 2, pp. 171–187, 1997.

[52] S. McCamish, M. Pachter, and J. D'Azzo, "Optimal formation flight control," in *Guidance, Navigation, and Control Conference*, p. 3868, 1996.

[53] M. Brodecki, K. Subbarao, and Q.-P. Chu, "Formation flight control system for in-flight sweet spot estimation," in *51st AIAA Aerospace Sciences Meeting including the New Horizons Forum and Aerospace Exposition*, p. 1037, 2013.

[54] Q. Zhang and H. H. Liu, "Aerodynamic model-based robust adaptive control for close formation flight," *Aerospace Science and Technology*, vol. 79, pp. 5–16, 2018.

[55] L. M. Milne-Thomson, *Theoretical aerodynamics*. Courier Corporation, 1973.